

©[2012]

Yi Xu

ALL RIGHTS RESERVED

PHYTOPLANKTON DYNAMICS STUDYING USING OBSERVATION AND BIO-
PHYSICAL MODELING

By

YI XU

A Dissertation submitted to the
Graduate School-New Brunswick
Rutgers, The State University of New Jersey

in partial fulfillment of the requirements

for the degree of

Doctor of Philosophy

Graduate Program in Oceanography

written under the direction of

Dr. Oscar M.E. Schofield

and approved by

New Brunswick, New Jersey

January, 2013

ABSTRACT OF THE DISSERTATION
PHYTOPLANKTON DYNAMICS STUDYING USING OBSERVATION AND BIO-
PHYSICAL MODELING

By YI XU

Dissertation Director:

Dr. Oscar M.E. Schofield

Continental shelf phytoplankton bloom dynamics are associated with meteorological, oceanographic and coastal forcing mechanisms. Mixing related to stratification and de-stratification is a key process of the physical environment that can control the timing and magnitude of blooms. Using data from satellite, coastal ocean observatory and bio-physical model, this study investigated the seasonal and decadal variability of chlorophyll in the Mid-Atlantic Bight and how different forcing mechanisms affect the phytoplankton bloom.

The temporal and spatial distribution of chlorophyll a in the MAB was quantified using satellite data collected by the Sea-viewing Wide Field of view Sensor (SeaWiFS). The MAB undergoes a fall-winter bloom in the middle-outer shelf region and spring bloom in the shelf-break region. The interannual variability of bloom magnitude is associated with wind-induced mixing.

Mixing has been recognized as having an important role in influencing underwater light and nutrient budgets and thus regulating phytoplankton bloom. The ratio of light over mixed layer depth (MLD) was used to determine the trade-off effects of mixing on phytoplankton bloom activity. We find that a critical light value around 60 (W m^{-2}) for the shelf region and 150 (W m^{-2}) for the shelf-break front region in promoting maximum phytoplankton biomass and there is a predictable linear regression relationship between the critical light value and depth.

The bio-physical model identified the wind-induced mixing, net heat flux and river run-off are the most important factors influencing water column stability. Sensitivity studies showed that the timing of the destratification and initiation of fall bloom was closely related to the wind forcing. The river's role in bringing buoyancy was significant in increasing phytoplankton bloom.

The decadal declines in the seasonal satellite estimates of chlorophyll a concentrations have been observed in the fall and winter in the MAB and are hypothesized to reflect shifts in the Atlantic Multidecadal Oscillation (AMO) that alters wind stress, river discharge, and net heat flux.

This work prototypes the integration of observation and modeling in a coastal environment and demonstrates the use of 3D coupled physical-biological model forced with realistic atmospheric forcing to study the phytoplankton dynamics in the MAB.

Acknowledgements

First and foremost, I would like to thank my advisor Dr. Oscar M.E. Schofield, for his guidance, encouragement and support throughout my time at Rutgers. I will never find the words to thank him for all his contributions of time, ideas, and mentoring and I much regret the fact that I will have little chance to pay him back for all his personal dedications. With his enthusiasm, his inspirations and his great effects to guide me to get everything planed and done in right way and in right time, he helped me to qualify myself for a PhD candidate as much as possible. In every sense, none of my PhD research work would have been possible without him. I am also thankful for the excellent example he has provided as a devoted, loyal, persistent and successful professional.

I would like to express sincere gratitude to my committee, Bronwyn Cahill, Bob Chant, Katja Fennel, and John Wilkin for their helpful comments and constant support. Their overseeing of my doctoral work and insightful comments on my dissertation improved this work substantially. I would like to acknowledge Dr. Robert Chant for his encouragement and the inspiring conversations we had over the years. Bob has always been supportive to my ideas. His sense of humor also made my time in IMCS much enjoyable. I am also very grateful to Dr. John Wilkin and Dr. Bronwyn Cahill for the guidance of using ROMS which made that experience much less painful.

I would also like to thank my colleagues at COOL lab not only enabled my study with their support and hard work but also made my study enjoyable: Dr. Josh Kohut who gave a lot of support of dealing with ocean observation data; Jennifer Bosch who is my initial guidance of using satellite data; Renato Castelao who bring me to the glider data analysis.

I am always very grateful that all faculties and graduate students in the Institute of Marine and coastal science. They are so friendly and very helpful all the time. With them, my PhD life has more joys and funs in both teaching and doing research.

Lastly, my tones of thanks must go to my family. Thank my wonderful parents Jincheng Xu and Guangying Wei who raised me and taught me with unreserved loves. Thanks to my husband Fei Song for everything he did for me. It's him who companied me through every stop of my PhD journey. And my loved son and daughter, Aiden Song and Willow Song. They bring me countless joys and happiness. I could not describe how grateful I am to have them during my PhD.

Table of Contents

ABSTRACT OF THE DISSERTATION	ii
Acknowledgements.....	iv
Table of Contents.....	vi
List of Tables	ix
List of Figures.....	x
CHAPTER 1. INTRODUCTION.....	1
CHAPTER 2. SEASONAL VARIBILITY OF CHLOROPHYLL A IN THE MID- ATLANTIC BIGHT	4
2. 1. Introduction.....	4
2. 2. Methods.....	6
2. 2. 1. Ocean color remote sensing data.....	6
2. 2. 2. Winds and surface current observations.....	9
2. 2. 3. River discharge and glider data	11
2. 2. 4. EOF and Cluster analysis	12
2. 3. Results.....	13
2. 3. 1. Seasonal cycle.....	13
2. 3. 2. Mechanisms underlying the inter-annual chlorophyll variability.....	19
2. 4. Discussion.....	21

CHAPTER 3. ROLE OF WIND IN REGULATING PHYTOPLANKTON BLOOMS ON THE MID-ATLANTIC BIGHT	38
3. 1. Introduction.....	38
3. 2. Methods.....	40
3. 2. 1. The Biogeochemical Model.....	40
3. 2. 2. Glider Observations.....	43
3. 3. Result	44
3. 3. 1. Model Simulation and Observations of MAB phytoplankton.....	44
3. 3. 2. Environmental regulation of phytoplankton.....	45
3. 3. 3. Light, upper mixed layer depth, and chlorophyll	49
3. 4. Discussion.....	51
CHAPTER 4. DECADAL VARIABILITY OF CLIMATE AND WINTER PHYTOPLANKTON BLOOM IN THE MID-ATLANTIC BIGHT	69
4. 1. Introduction.....	69
4. 2. Data, Model, and Methods	71
4. 3. 1. Ocean color remote sensing data.....	71
4. 3. 2. Meteorology data.....	72
4. 3. 3. Biogeochemical Model.....	72
4. 3. Results.....	73
4. 3. 1. Terms influencing water column stability.....	73

4. 3. 2. Model sensitivity study.....	75
4. 3. 3. Decadal variability of Chlorophyll	76
4. 3. 4. Decadal variability of Meteorological Forcing.	77
a. Wind.....	77
b. Temperature, salinity and net heat flux.....	78
c. River discharge	79
4. 4. Conclusion.....	81
CHAPTER 5. CONCLUSIONS	91
REFERENCES	93
Curriculum Vita	101

List of Tables

Table 2. 1. Chlorophyll (mg m^{-3}) and light environment for the two regions defined by the EOF analysis in the MAB. For the shelf waters the 1% light depth was calculated using Hydrolight combined with optical data collected during the LaTTE experiment (Chant et al., 2008b, Moline et al., 2008). 27

Table 4. 1. Percentage change of wind, river, net heat flux and chlorophyll from AMO- period to AMO+ period. Positive means increase, negative means decrease..... 83

List of Figures

- Figure 2. 1. Map showing study area, NDBC mooring stations, and glider track. Topographic contours shown are 40, 60, 80, 150, and 1000 m. Gray shaded area indicates location where SeaWiFS imagery was analyzed. 28
- Figure 2. 2. Number of images used each in month for the entire time series of 4-day chlorophyll composites. 29
- Figure 2. 3. Monthly mean chlorophyll (mg m^{-3}) from January 1998 to December 2006 for MAB (shaded gray area in Figure. 1). The numbers on the top indicate the relative percentage of annual mean chlorophyll for each month. 29
- Figure 2. 4. The EOF modes for chlorophyll in MAB. Left panels are the first two EOF modes, right panels are percentage of the local variance explained by each mode. 30
- Figure 2. 5. Time series of the amplitude of the first two EOF modes. 31
- Figure 2. 6. Vertical sections of glider transect. Salinity (left), temperature (middle) and backscatter (right) collected along the Rutgers Glider Endurance line (See Figure. 1 for location; Schofield et al., 2007) during winter (top) and spring (bottom). 32
- Figure 2. 7. Monthly climatology of SST (thin black line, $^{\circ}\text{C}$), PAR (dash line, Einsteins $\text{m}^{-2} \text{day}^{-1}$) and chlorophyll (thin line with dot, mg m^{-3}) averaged over the two regions (Zone 1 and Zone 2 in Figure. 4) identified by the EOF analysis. Value averaged over Zone 1 is shown on panel (A) together with correlation coefficient between cross-shelf wind and cross-shelf current (bold black line). Value averaged over Zone 2 is shown on

panel (B), together with correlation coefficient between along-shelf wind and along-shelf current. In both panels, correlation analysis used wind observations from NDBC 44009 station, and HF radar currents along the cross-shelf line which is coincident with the glider endurance line (See Figure. 1 for location) 33

Figure 2. 8. Seasonal Surface current on the New Jersey Shelf (cm s^{-1}), vectors represent the current field and the color map is the magnitude of velocity: (A) Winter (December - February) (B) Spring (March - May)..... 34

Figure 2. 9. Monthly and special averaged chlorophyll concentration (gray line) for area (Zone 1 in Figure. 4(B)) depicted by the EOF mode 1 (mg m^{-3}). The triangle marked black line represents the monthly mean river discharge in $\text{m}^3 \text{s}^{-1}$ 35

Figure 2. 10. (A) SeaWiFS chlorophyll 4-day composite image (January 25th to 28th, 2006). The white line on this panel indicates the location of the glider transect. (B) Salinity cross-section measured with a glider along the transect shown in panel (A). The glider measurement is from 2006 January 18th to 23rd 36

Figure 2. 11. (A) Percentage of stormy days against maximum SeaWiFS chlorophyll concentration (mg m^{-3}) in the area depicted by EOF mode 1, (B) Percentage of stormy days against maximum SeaWiFS chlorophyll concentration (mg m^{-3}) in area depicted by EOF mode 2. In panel (A), wind observations are from NDBC 44025 during Dec. to Jan., while in panel (B), winds are from NDBC 44014 during Feb. to Mar.; the star for 2003 means we consider it as an outlier. 37

Figure 3. 1. Model domain (light grey). Dark grey and grey highlight the Zone 1 and Zone 2 region identified by Xu et al. (2011). Red and green lines show the glider transects. Red and green square symbols represent the grid point used for calculation in Zone 1 and Zone 2. The black lines with number show the bathymetry. 56

Figure 3. 2. The nine-year record of SeaWiFS chlorophyll (bar) compared to photosynthetically active radiation (PAR, blue line) from the spatial mean in (A) Zone1 and (B) Zone2. The black line overlapped is the model simulated spatial mean chlorophyll in Zone 1 and Zone 2. 57

Figure 3. 3. Time series of surface chlorophyll concentration (black line) and net heat flux (grey line) of spatial mean in Zone 1 and Zone 2 calculated from model output. 58

Figure 3. 4. Comparison between the log-transformed surface chlorophyll concentrations provide by SeaWiFS and mode output from spatial mean of Zone 1 and Zone 2. The linear correlation of the chlorophyll before log-transformed is 0.42 and 0.75 (P value <0.001) for Zone 1 and Zone 2 respectively. The climatology of surface water temperature from the NDBC buoy 44009 (the red line with error bar) was used to compare with the simulated SST at the same location (blue line) in Figure 4C. 59

Figure 3. 5. Model simulated vertical distribution of temperature (A) chlorophyll concentration (B), light (C), NO₃ (D) and zooplankton (E) at a point located in Zone 1 (dot shown in Figure 1). The 1% light level depth is plotted with light (in C, red line) and the MLD is plotted with NO₃ (in (D), white line). 60

Figure 3.6. Model simulated vertical distribution of temperature (A) chlorophyll concentration (B), light (C), NO₃ (D) and zooplankton (E) at a point located in Zone 2 (square shown in Figure 1). The 1% light level depth is plotted with light (in C red line) and the MLD is plotted with NO₃ (in D, white line). (Here, we only show the upper 150 m of the water column). 61

Figure 3. 7. Vertical distribution of limitation function of light (A) and nutrient (B) at a point located in Zone 1 (dot shown in Figure 1). The 1% light level depth is plotted with function of light (in A, red line) and the MLD is plotted with nutrient limitation function (in (B), green line)..... 62

Figure 3. 8. Spatial mean chlorophyll in Zone 1 under different scale of wind 63

Figure 3. 9. Simulated time series of spatial mean surface chlorophyll concentration in Zone 1(A) and Zone 2(B). Black line represents the result under normal wind conditions; grey line represents the “no wind” forcing result. 63

Figure 3. 10. Without wind forcing, the simulated vertical distribution of temperature (A) chlorophyll concentration (B), light (C), NO₃ (D) and zooplankton (E) in a dot located in Zone 1(dot shown in Figure 1). The 1% light level depth is plotted with light (in C, red line) and the MLD is plotted with NO₃ (in (D), white line)..... 64

Figure 3. 11. Difference (normal wind – no wind) of mixed layer mean light (black line) and nutrient (gray dashed line) limitation function between normal wind and no wind forcing condition in (A) Zone 1 and (B) Zone 2. For Zone 1, negative light function

difference value in winter represents the decrease of light limitation under no wind condition.	65
Figure 3. 12. Scatter plot of modeled mean light value in the mixed layer with MLD in Zone 1 (a) and Zone 2 (b). The color represents the chlorophyll concentration (mg m ⁻³).	66
Figure 3. 13. Simulated mixed depth mean chlorophyll concentration and I' in every 20 W m ⁻² . I' value bins in Zone 1 (grey circle line) and Zone 2 (grey plus line), chlorophyll and I' based on glider observation are shown in black line with dots.	66
Figure 3. 14. The critical light value ($I'_{chl\ max}$) in each grid of model domain.	67
Figure 3. 15. The relationship between the critical light value and water depth of all grids in the MAB. We separate grids in Zone 1 and Zone 2 with circle and triangle individually. Black line represents the linear regression of water depth and critical light value.....	68
Figure 3. 16. Under no wind forcing, simulated mixed depth mean chlorophyll concentration and I' in every 20 W m ⁻² . I' value bins in Zone 1 (red circle line) and Zone 2 (blue circle line), chlorophyll and I' based on glider observations are shown in black line with dots.....	68
Figure 4. 1. Time serials of change of PEA with time in equation (9).	84
Figure 4. 2. Model sensitivity study results of the time serials of Zone 1 spatial mean PEA (a) and chl a (b) under different forcing. In the Experiment of ‘no wind’ and ‘no net	

heat flux’, the wind and net heat flux are turned off at the day (around the 282 day of year 2005) when the neat heat flux changes from positive to negative (Here we only compare the results after that day). The normal condition results are shown in black line. In the PEA lot, the black line is overlapped partially with the no river condition in winter; in the chl a plot, the black line is overlapped with no river nutrients input condition (light blue line). 85

Figure 4. 3. Decadal variability of chl a. (a) Monthly average chl a anomalies, blank window means there is no available data at this month. (b) Climatological seasonal cycles in chl a (black), their standard deviation (gray shading), AMO+ composites (red dashed line), and AMO- composites (blue dashed line). (c) Spatial coefficients of EOF mode 1. (d) CZCS-SeaWiFS chl a time variability of EOF mode 1 (black). AMO index is superimposed as gray shading. 86

Figure 4. 4. Winter time storm frequency for the NDBC buoys 44008, 44011, 44025, and 44009..... 87

Figure 4. 5. The climatology of storm frequency of 44008 and 44009 NDBC moored buoys(a,b) and NCEP data at the same location (c,d)for those two time periods..... 88

Figure 4. 6. The NCEP climatology temperature and salinity difference in January for the time period 1983-1986 and 2004-2008. a) temperature; b) salinity 88

Figure 4. 7. The climatology water and air temperature of 44009 NDBC moored buoys for the time period of 1983-1986 and 2004-2008. 89

Figure 4. 8. The climatology of river discharge for the time period of 1983-1986 and 2004-2008. 89

Figure 4. 9. Normalized anomalies of river, net heat flux and wind. The data are normalized by dividing the standard deviation of the time series. The AMO index is superimposed as green line. The year 1995 (vertical green line) is the division between the AMO- and AMO+..... 90

CHAPTER 1. INTRODUCTION

In many parts of the world's ocean the annual cycle of phytoplankton growth is dominated by a rapid seasonal increase most often exhibited as spring bloom. The classic description of the conditions necessary for phytoplankton bloom initiation were developed by Sverdrup (1953) for the subpolar North Atlantic. Deep mixed layers and low solar radiation during winter reduce the mean light available to phytoplankton to a level below that required for growth. Increasing incident light and reduced mixing in spring result in the mixed layer shallowing beyond a "critical depth" where the average light intensity is such that phytoplankton growth exceeds losses, so the spring bloom begins. This critical depth concept was first challenged by Townsend et al. (1992) and Eilertsen (1993) who reported that the phytoplankton spring bloom happened before the onset of vertical stratification in the Gulf of Maine and in several Norwegian fjords with water depths of >200m developed in the absence of vertical stratification. A new theory developed by Huisman et al. (1999) that blooms can occur even in the absence of vertical stratification, as long as the vertical turbulent mixing rates are less than certain critical level. On a basin scale, the bloom dynamics involve the balance between nutrient entrainment and light limitation. Strong mixing supplies nutrients to surface waters for phytoplankton growth while simultaneously limiting light availability at depths. Dutkiewicz et al. (2001) showed that vertical mixing in the upper-ocean boundary layer can increase productivity in the subtropical region but can also decrease productivity due to the mixing of phytoplankton below the critical depth. In the subtropical region where there is no light limitation, increased mixing during the bloom period supplies nutrients from deep waters to the upper ocean, thus having a positive effect on phytoplankton

blooms (Dutkiewicz et al., 2001; Follows and Dutkiewicz, 2002). So, the water column stability which influences light and nutrient availability have significant influence on the phytoplankton dynamics.

The Middle Atlantic Bight (MAB) lying between the subpolar and subtropical regimes is a transition zone includes the coastal and shelf areas from Nantucket Shoals off the southern Massachusetts coast to Cape Hatteras, North Carolina. The MAB is a complex ecosystem that is strongly influenced by the physical oceanography and meteorology of the region. Shelf water originates from the coast of Newfoundland that mixes with various riverine input along the way and bounded on the offshore side by the slope sea and the Gulf Stream western boundary current. It has long been appreciated that seasonal phytoplankton blooms are important in shelf and slope waters of the MAB (Riley, 1946; 1947; Ryther and Yentsch, 1958). As the physical regulation of water column turnover is spatially variable along the MAB, the temporal patterns in phytoplankton biomass are not always spatially coherent within the East Coast shelf/slope ecosystem (Yoder et al., 2001). Seasonal and inter-annual variability in spatial extent, timing and magnitude of the phytoplankton bloom is in part driven by the physical forcing. The water in the Middle Atlantic Bight (MAB) undergoes significant decadal variability in the temperature, salinity. Based on the hydrographic data during the period 1997-1999 from the Northeast Fisheries Science Center (NEFSC) MARMAP program, Mountain (2003) have shown that there is a 1°C warmer and 0.25 PSU fresher of MAB shelf water in the 1990s than the 1977-1987 period. Long records (1875–2007) of temperature data over the US continental shelf along the east coast indicate that there is substantial interannual variability of temperatures arises due to advection from the north

(Shearman and Lentz, 2010). Some of this variability is associated with the Atlantic Multidecadal Oscillation (AMO) which is an index based on the variations of the sea-surface temperature in the North Atlantic with characteristic time scales of 50–100 yr. Assessing if the seasonal patterns of phytoplankton bloom in the MAB have changed is an open question, as for the continental shelf of MAB, very few sufficiently long term biological time series exist to assess interannual to decadal variability of phytoplankton bloom. Although it is not possible to detect decade-scale variability by using the longest currently-operating Sea-viewing Wide Field of view Sensor (SeaWiFS) data alone, by comparing climatological SeaWiFS data against data from the CZCS, which operated between 1979 and 1985 can be a way to detect long-term trends in marine biology due to climate change. Understanding past variability in bloom dynamics and the associated physical mechanisms is a key to predict how ocean biology will respond to climate change.

My dissertation focuses on characterizing the seasonal phytoplankton bloom in the MAB and the decadal variability of blooms in the different climate weather condition. The combination of observation and bio-physical model is used to understanding the underlying mechanism regulating the phytoplankton bloom dynamics.

CHAPTER 2. SEASONAL VARIABILITY OF CHLOROPHYLL A IN THE MID-ATLANTIC BIGHT

2. 1. Introduction

The Mid-Atlantic Bight (MAB) is a biologically-productive continental shelf that is characterized by consistently high chlorophyll biomass ($>1 \text{ mg chlorophyll m}^{-3}$) which supports a diverse food web that includes abundant fin and shellfish populations (Yoder et al., 2001). The MAB's shelf extends out for several hundred kilometers and the associated water mass is bounded offshore by the shelf-break front. While the shelf-break front is often near the geological shelf-break, the surface outcrop of the front can extend beyond the continental slope (Wirick 1994). In the nearshore regions there are numerous inputs from moderately sized, yet heavily urbanized, rivers (Hudson River and Delaware River), which are sources of fresh water, nutrients, and organic carbon to the MAB (O'Reilly and Busch, 1984). The waters on the MAB exhibit considerable seasonal and inter-annual variability in temperature and salinity (Mountain, 2003). In late spring and early summer, a strong thermocline (water temperatures can span from 30° to 8° C in <5 meters) develops at about the 20 m depth across the entire shelf, isolating a continuous mid-shelf "cold pool" (formed in winter months) that extends from Nantucket to Cape Hatteras (Houghton et al., 1982, Biscaye et al., 1994). The cold pool persists throughout the summer until fall when the water column overturns and mixes in the fall (Houghton et al., 1982), which presumably replenishes nutrients to the surface waters on the MAB shelf. Thermal stratification re-develops in spring as the frequency of winter storms decrease and surface heat flux increases (Lentz et al., 2003).

In temperate seas, seasonal phytoplankton variability has been related to stratification, destratification and incident solar irradiance (Cushing, 1975; Longhurst, 1998; Dutkiewicz et al., 2001; Ueyama and Monger, 2005). During late winter and early spring, increasing solar illumination combined with decreasing wind result in shallower surface mixed layers which allows for increased phytoplankton growth prior to the development of the thermal stratification (Stramska and Dickey, 1994; Townsend et al., 1994). As the physical regulation of water column turnover is spatially variable along the MAB, the temporal patterns in phytoplankton biomass are not always spatially coherent within the East Coast shelf/slope ecosystem (Yoder et al., 2001). While it has long been appreciated that seasonal phytoplankton blooms are important in shelf and slope waters of the MAB (Riley, 1946, 1947; Ryther and Yentsch, 1958), a 7.5-year (October, 1978 to July, 1986) time series of the coastal zone color scanner (CZCS) imagery found that the maximum chlorophyll concentration appeared during fall-winter on the continental shelf waters and that slope waters possessed a secondary spring peak in addition to a fall-winter bloom (Yoder et al., 2001). Ryan et al. (1999) used CZCS imagery from 1979 to 1986 and found an annual enhancement of chlorophyll at the shelf-break of the MAB and Georges Bank during the spring transition from well-mixed to stratified conditions. The shelf-edge system was similar to inner shelf waters in terms of seasonal heating and cooling, however meanders at the shelf slope were associated with iso-pycnal upwelling that supplied nutrients to the euphotic zone and enhanced chlorophyll biomass (Ryan et al. 1999). Despite past efforts, understanding what regulates the magnitude of these seasonal patterns remains an open question, which is especially important as the MAB has

experienced significant changes in water properties over the last few decades (Mountain, 2003).

Many factors are known to regulate the upper mixed layer dynamics on the MAB. These features include wind driven mixing (Beardsley et al., 1985) as well as surface buoyant plumes that frequently extend over significant fractions of the MAB shelf (Castelao et al., 2008a; Chant et al., 2008a). These features are superimposed upon the seasonal warming that drives the stratification of the MAB. This seasonality of shelf stratification regulates the phasing and potential magnitude of the fall-winter and spring enhancements in chlorophyll concentration. For this manuscript we use a 9-year time series of Sea-viewing Wide Field of view Sensor (SeaWiFS), HF radar, and Webb Glider data to assess the physical forcing of the seasonal and inter-annual variability of the spatial distribution in phytoplankton.

2. 2. Methods

2. 2. 1. Ocean color remote sensing data

Time series of surface chlorophyll concentration in the MAB was studied using 4-day averaged composites of SeaWiFS satellite imagery collected from January 1998 to December 2006. We used 4-day average composites as they provided reasonable coverage for our study site and could resolve the dynamics of the chlorophyll over both seasonal and higher frequency scales (days to weeks) often observed in MAB. The 4-day average decreased the cloud contamination that heavily degraded the utility of the 1-day images. Many phytoplankton bloom events occur over time scales much shorter than a month in these waters. For example chlorophyll associated with buoyant plume events can last for the time scale of 4-5 days (Moline et al. 2010, Schofield et al. submitted) and

summer upwelling on average lasts for <7 days in the MAB (Glenn et al. 2004). Longer term averaging underemphasizes these shorter-lived phytoplankton bloom events that can explain up to 44% of the variability observed in daily satellite imagery (Yoder et al.,2001). The spatial resolution of the original images were 1.1 km, however, data were re- gridded to 5.5 km in order to identify the principal modes of variability in the dataset by Empirical Orthogonal Function (EOF) analysis. Given the high spatial heterogeneity in the nearshore waters and the increasing error in satellite estimates of chlorophyll in shallow waters, we excluded regions with water depths shallower than 10 m for this analysis. We also excluded data for water depths deeper than 2000 m, as our focus was on the shelf and shelf-break region. Finally we excluded data from large inland Bays (Long Island Sound, Delaware Bay and Chesapeake Bay) (Figure.2.1). Monthly chlorophyll concentration was calculated by taking the geometric mean at each pixel. We chose to use the geometric rather than the arithmetic mean because the distribution of chlorophyll measurements in continental shelf and slope waters is approximated by a log-normal distribution (Campbell, 1995; Yoder et al., 2001).

Ocean color satellite remote sensing has limitations in coastal waters. Satellite coverage is limited by cloud cover especially in the winter months, which is characterized by frequent storms. Storms also can produce buoyant plumes that contain significant amounts of sediment and colored dissolved organic matter. The presence sediment and CDOM can influence the accuracy of the satellite-derived estimates of chlorophyll that can result in errors as large as 50-100% in the near-shore waters of the northeast United States (Harding et al. 2004). Finally, ocean color remote sensing does not provide information on subsurface phytoplankton peaks, below the detection limit of the satellite,

which are often present in the MAB. While we acknowledge these shortcomings, satellite estimates of chlorophyll remains one of the only techniques that can provide decadal spatial time series over ecologically relevant scales.

We also calculated the monthly climatological sea surface temperature (SST) for each pixel based on 4-day averaged Advanced Very High Resolution Radiometer (AVHRR) data sets from 1999 to 2006. The AVHRR data sets were collected by a satellite dish maintained by Rutgers University Coastal Ocean Observation Lab and processed using SeaSpace AVHRR processing software. Monthly SeaWiFS Level 3 photosynthetically available radiation (PAR) data from 1998 to 2006 were downloaded from <http://oceancolor.gsfc.nasa.gov>. The PAR data sets have the resolution of 9 km and the climatology of PAR was calculated based on the 9-year monthly data sets.

The mean satellite derived chlorophyll fields were used as inputs to the Hydrolight 4.3 radiative transfer model (Mobley, 1994) to estimate the depth of the 1% light levels. For the Hydrolight simulations, we used default settings and assumed a constant backscatter to total scatter ratio of 0.05 based on data collected in this region (Moline et al., 2008). We assumed there was no inelastic scattering and kept wind speeds at zero. The surface flux of light was calculated using a semi-empirical sky model (Mobley, 1994) for the MAB at local noon on a cloudless day. We assumed that water column was infinitely deep. These Hydrolight simulations assumed no vertical structure in the phytoplankton biomass. We used this approach even though during the stratified season there can be subsurface chlorophyll layers (Schofield et al. 2009), however satellite derived chlorophyll estimates were used as the input to the Hydrolight simulation and these estimates are exponentially weighted to the surface waters (Mobley 1994);

therefore it is unlikely that satellite estimates included any significant proportion of the subsurface populations found at the base of the pycnocline in the late spring and summer months. Given this we did not impose a vertical structure for chlorophyll. For these simulations we treated the MAB as Case I waters (Johnson et al., 2003). This assumption is sometimes not the case when the Hudson River carries significant amounts of detritus and colored dissolved organic matter (CDOM) offshore onto the MAB (Johnson et al., 2003). Despite the optical complexity of these waters, SeaWiFS can accurately and reliably capture seasonal and inter-annual variability of chlorophyll a associated with variations of freshwater flow (Harding et al., 2005), which can increase chlorophyll biomass by an order of magnitude. To assess the impact of Case II conditions on our Hydrolight estimates of the 1% light depth, we used optical data collected as part of the LaTTE experiment (Chant et al., 2008b), which in part focused on characterizing the optical properties of the Hudson River waters being transported out onto the MAB (Moline et al., 2008). During the LaTTE experiment, data were collected in the Hudson River outflow over time with a WETLabs, Inc. absorption/attenuation meter using the methods outlined in Schofield et al., (2004). The waters influenced by the Hudson River, which was characterized by significant contributions of chlorophyll and CDOM providing Case II waters. These measurements of the optical properties were inputted into the Hydrolight model to provide an estimate for light propagation in the Case II characteristics for MAB waters.

2. 2. 2. Winds and surface current observations

Wind data were obtained from moored buoys deployed by the National Data Buoy Center (NDBC) (<http://www.ndbc.noaa.gov/maps/Northeast.shtml>). We used data

collected by mooring 44025 (Figure. 2.1) located at 40.25°N , 73.17°W with a water depth of 36 m and mooring 44014 (Figure. 2.1) located at 36.61°N , 74.84°W with a water depth of 48 m. The reason we chose these two moorings was because 44025 was located at the mid-shelf region while 44014 was located at shelf-break/slope region. We used the daily wind speed data to calculate the storm frequency. The wind data used for calculating the correlation coefficient between the surface currents measured by CODAR and wind speed were based on the time series of the 6 years (2002 to 2007) wind measured at NDBC 44009 (Figure. 2.1) located at 38.46°N , 74.70°W with a water depth of 28 m. We used this mooring as it was central to a recently completed long-term analysis of the circulation on the MAB (Gong et al., 2010). The wind data for 44009 were decomposed into along-shelf and cross-shelf directions (30 degree rotation) and low-passed with a 33- hour filter. Shore-based High Frequency (HF) radar systems were used for surface current measurements. The radar network was a fully nested array of surface current mapping radars (Kohut and Glenn, 2003; Kohut et al., 2004). Hourly surface currents were measured with an array of CODAR HF Radar systems consisting of 6 long-range (5 MHz) and 2 high-resolution (25 MHz) backscatter systems from the start of 2002 to the end of 2007. For all systems measured beam patterns were used in surface current estimates (Kohut and Glenn, 2003). Details of HF radar development and theory can be found in (Crombie, 1955; Barrick, 1972; Stewart and Joy, 1974; Barrick et al., 1977). All CODAR surface currents were de-tided using the T_TIDE Matlab package (Pawlowicz et al., 2002) before further analysis is performed. The averaged seasonal surface current responses for the dominant winds were calculated for the well-mixed

winter (December- March), the transitional seasons (April-May, October-November), and stratified summer (June-September) (Gong et al. 2010).

2. 2. 3. River discharge and glider data

The monthly river discharge data were downloaded from <http://nwis.waterdata.usgs.gov/nwis>. The total river discharge into to the MAB was represented by the sum of the discharges from Mohawk River at Cohoes, NY (42.79°N, 73.71°W), Passaic River at Little Falls, NJ (40.89°N, 74.23°W), Raritan River below Calco Dam at Bound Brook, NJ (40.55°N, 74.55°W), Hudson River at Fort Edward, NY (43.27°N, 73.60°W) and Delaware River at Trenton, NJ (40.22°N, 74.78°W).

Webb Slocum gliders were used to obtain subsurface measurements over the shelf. The Webb gliders occupy a cross-shore transect across the MAB beginning in 2005 (Schofield et al 2007); however, the coverage in each month is not always complete. The cross-shelf transects typically take on average 4-5 days and are appropriate for comparing to the 4-day averaged satellite imagery. The cross shore transect typically spans the 15 to 100 m isobaths (Figure. 2.1). The gliders were outfitted with CTDs (Sea-Bird Electronics, Inc.) and occasionally with optical backscatter sensors (WETLabs, Inc.). For this effort we were able to utilize the data collected from nineteen cross-shore transects; however the coverage was not uniform over the year. There were 7 transects available during the fall and winter; however many of the early transects consisted of a glider that was not outfitted with a fluorometer or a backscatter sensor. Only 2 of 7 transects in fall and winter had any optical sensors present on board. Unfortunately no fluorometry data is available for the winter season and only one transect had only partial data of optical backscatter. There were twelve transects that were available for both the spring and

summer and all the gliders were outfitted with optical backscatter and chlorophyll fluorometers. We compared individual transects and to specific satellite imagery and also averaged the glider observations (Castelao et al., 2008b). While the glider data were sparser than the satellite and CODAR data, it represented the densest concurrent subsurface data available for the MAB.

2. 2. 4. EOF and Cluster analysis

EOF analysis is the mapping of the multi-dimensional data sets onto a series of orthonormal functions and is useful in compressing the spatial and temporal variability of large data sets down to the most energetic and coherent statistical modes. EOF results can be quite informative, however they that do not necessarily demonstrate causality and should be interpreted with caution. This method was first applied by Lorenz (1956) to develop the technique for statistical weather prediction. These approaches have been extremely useful for analyzing ocean color images, which have long time series and significant spatial variability (Baldacci et al., 2001; Yoder et al., 2001; Brickley and Thomas, 2004; Navarro and Ruiz, 2006). As EOF requires data sets without spatial gaps, we only used images that had less than 20% of pixels removed because of clouds. Additionally, prior to performing EOF analysis, any gaps in the data, due to clouds, were replaced by the average of the surrounding 8 non-cloud pixels. Using the criteria of less than 20% cloud cover, our final data set resulted in total of 468 4-day composites images with sufficient temporal resolution to resolve short-lived chlorophyll events. The numbers of images in each month used in the EOF analysis are presented in Figure. 2.2. EOF analysis was performed after subtracting the temporal mean of each pixel over the entire time series.

Additionally, we analyzed the chlorophyll variability using a cluster analysis. This was used to assess to what degree the different environmental conditions were associated with the chlorophyll concentrations over the 9-year data sets. Cluster analysis was carried out using Ward's method to minimize the sum of the squares of any two hypothetical clusters that can be formed at each step (Ward, 1963) in order to emphasize the homogeneous nature of each cluster. The cluster analysis was conducted using storm frequency, maximum chlorophyll concentration and mean river discharge during winter time (Dec. to Jan.) and carried out in SAS 9.1. The cluster analysis was complemented with regression analysis based on storm frequency, maximum chlorophyll concentration and mean river discharge.

2. 3. Results

2. 3. 1. Seasonal cycle

For the MAB (shaded gray area in Figure. 2.1), the spatially averaged monthly chlorophyll concentration revealed an annual cycle characterized by high values during fall-winter (October-March), which decreased until it reached lowest values during the highly stratified summer (Figure. 2.3). The integrated chlorophyll from October to March represented 58% of the annual chlorophyll. The fall-winter peak in chlorophyll began in the late fall and it persisted throughout the winter into early spring of the next year. The enhanced phytoplankton biomass in the fall-winter was most obvious in 2005 when there were high chlorophyll concentrations in November which remained high until March 2006. There was significant inter-annual variability in the magnitude of the fall- winter events, for example in 2002-2003 the fall-winter chlorophyll biomass was not as elevated as in the other years of this study.

The significance of the EOF modes for the spatial and temporal variability in chlorophyll was tested following methods described by North et al. (1998). The error produced in the EOF due to the finite number of images was $\delta\lambda \approx \lambda \left(\frac{2}{n}\right)^{1/2}$, where, λ is the eigenvalue and n is the degree of freedom. Only the first two modes were found significant. Spatial coefficients are presented in Figure. 2.4a and c. The color of the coefficient is directly related to the amplitude of the spatial coefficient. Temporal amplitudes of the EOF modes are presented in Figure. 2.5a. Therefore, the combination of the spatial and temporal variability can be obtained multiplying the spatial coefficient by the temporal amplitude. In our case, the first mode (Figure. 2.4a) explained 33% of the total variance, and was related with the seasonal enhanced chlorophyll in the fall-winter. It explained most of the variance between the 20 and 60 m isobaths. All the spatial coefficients were positive with the maxima found nearshore and decreasing offshore. Consequently, when they were multiplied by positive temporal amplitudes the whole field increased with respect to the chlorophyll climatology. The temporal amplitude with a 4-day interval showed high values in the fall-winter almost every year. Sometimes, there was a small increase of temporal amplitude in summer when the overall chlorophyll concentration was low ($<1 \text{ mg m}^{-3} \text{ Chl}$) except for the nearshore waters ($< 30 \text{ m}$ water depth) where summer upwelling is common (Glenn et al., 2004). The spatial and temporal coefficients suggested that in the middle and outer shelf the fall-winter enhanced chlorophyll was dominant.

The satellite derived EOF Mode 1 was consistent with the available glider observations (Figure. 2.6). The average sections for salinity (Figure. 2.6a), temperature (Figure. 2.6b) and optical backscatter (Figure. 2.6c) for the winter season showed very

little vertical structure, although there was a significant cross-shore gradient. Salinity increased with distance offshore with highest values beyond 60 kilometers from shore (Figure. 2.6a). Associated with the inshore lower saline waters were optical backscatter values that were 4-5 folds higher than those found in the offshore waters. The cross-shore extent of high backscatter values corresponded to the boundaries of satellite EOF Mode 1 (near 60 m isobaths) along the glider transects; however it should be noted that the optical backscatter measurements are also sensitive to the presence of sediments and plankton; however the lack of vertical structure in the glider optical data suggests that the winter satellite chlorophyll estimates are not biased by the subsurface layering in the phytoplankton populations.

The second EOF mode (Figure. 2.4c) explained 8% of the normalized variance and the spatial variability in mode 2 identified two different zones. The first zone had negative spatial coefficients and was located in the coastal areas within the 60 m isobath. The second zone had positive spatial coefficients located between the 80 to 150 m isobaths and extended to the MAB shelf-break front (Linder and Gawarkiewicz, 1998). Given this, the second mode applied to depths greater than 80 m and explained up to 32% of the chlorophyll local variance at those locations (Figure. 2.4d). The amplitude time series of the second EOF mode (Figure. 2.5b) generally showed positive values during spring, so when multiplied by positive spatial coefficients (yellow and red region in Figure. 2.4c) the whole field indicated an increase in the chlorophyll concentration over the shelf-break/slope during spring. Vice versa, the negative amplitudes multiplied by negative spatial coefficients (dark blue region in Figure. 2.4c) indicated that chlorophyll concentration increased such as seen in New Jersey and Long Island coastal areas during

the summer months in 2001 and 2002. The increases of chlorophyll concentration in the shallow coastal area during summer might be correlated with upwelling events. Our results confirm the conclusion in Glenn et al., (2004) that the coastal regions of New Jersey in the summer of 2001 had one of the most significant upwelling events over the 9-year records (1993-2001) (Moline et al 2004), which resulted in high phytoplankton biomass. Mode 2 also exhibited enhanced chlorophyll in the fall both on the shelf and over the continental slope. The spring glider observations did exhibit enhanced particle concentrations (as detected by the optical backscatter data), both in nearshore (shallower than 30 m) and offshore (deeper than 80 m) waters (Figure. 2.6c, bottom panel). The enhanced particle concentrations in offshore waters were detectable during the spring, consistent with the EOF mode 2 measured by satellite. In contrast to the winter months, the spring optical data showed significant vertical heterogeneity, with the highest values found at depth. The enhanced backscatter values have been related to storm/wave/tidally driven resuspension processes (Glenn et al., 2008). The enhanced sea surface optical backscatter was associated with increased water column salinity (Schofield et al. 2009). Low salinity water consistently had higher backscatter values in the surface (Figure. 6a, c, bottom panel).

The chlorophyll climatology in the MAB was analyzed for the two spatial zones delineated by the EOF analysis. The middle and outer shelf region (Zone 1 enclosed in Figure. 2.4b where the local variance were larger than 40%) identified by the first EOF mode showed mean chlorophyll concentration that ranged between 1.3-2.3 mg m⁻³ with highest values observed in fall-winter, and lowest values observed during summer (Figure. 2.7a, dotted thin line). The highest chlorophyll values were inversely related to

the seasonal cycle of PAR and SST, which were highest in June and August respectively. There was a two-month phase lag between PAR and SST. The measured PAR values would lead to light limitation in phytoplankton photosynthesis based on the available photosynthesis-irradiance measurements (Schofield et al. in review).

Six years of surface HF radar current data showed that during winter the mean surface flow on the New Jersey shelf was generally offshore and down-shelf (Figure. 2.8a). Based on wind data from NDBC moored buoy 44009, winter was characterized by strong northwest winds, which we define as a mean velocity of 9.1 m s^{-1} and occur 39% of the time (Gong et al., 2010). Based on the extensive spatial and temporal analysis conducted in Gong et al. (2010), we analyzed the correlations between winds and surface transport during the winter. The cross-shelf wind and cross-shelf surface currents had strong correlations ($R^2 > 0.7$) during the late fall and winter (Figure. 2.7a, black bold line). Since winds were predominantly from the northwest in winter, cross-shelf flow was observed during this time (Figure. 8a, Gong et al. 2010). The strong northwest winds thus increased the transport of inner shelf fresh and nutrient rich water across the middle of the shelf (Gong et al. 2010). As this occurred when chlorophyll concentrations were high (Figure. 2.7a, thin line with dot), we hypothesize that the cross-shelf transport of fresh water induced intermittent surface stable layer, that promoted phytoplankton growth. Moreover, the cross-shelf transport may carry coastal phytoplankton populations from the nearshore (<20 m depths) out across the areal extent of EOF zone 1. Therefore, the highest phytoplankton concentrations occurred when the cross-shelf currents were correlated with cross-shelf wind in the late fall and winter. Simulations using passive particle tracers support this interpretation (Gong et al. 2010).

The second EOF mode explained more than 25% of the variance at the shelf-break/slope region (Zone 2 enclosed in Figure. 2.4d). The spatially averaged chlorophyll concentration in Zone 2 exhibited a maximum chlorophyll concentration in spring that fluctuated between 0.3 and 1.5 mg m⁻³ over the year. Chlorophyll concentrations began to increase as PAR began to increase. The chlorophyll concentration began to decline as SST began to increase late in spring. The second peak of chlorophyll concentration appeared in fall with a peak of 0.9 mg m⁻³ as climatological means of PAR and SST began to decrease.

The six-year climatology of seasonal flow on the shelf during spring was mostly down-shelf towards the southwest (Figure. 2.8b). Northeast (along-shelf) winds were more common in spring and fall. The response of surface flow under northeast winds was most energetic during the transition seasons (Gong et al. 2010). Therefore, the high correlation coefficient between along-shelf wind and along-shelf current appeared during the transitional periods (April-May and October-November) (Figure. 2.7b, black bold line), when the water column was stratifying in spring and as stratification was eroded in fall. The northerly winds potentially bring up shelf bottom boundary layer water through shelf break upwelling, which is a source of nutrients and could contribute to enhanced chlorophyll in spring and fall (Siedlecki et al., 2008).

In EOF Zone 2, there was another small peak of chlorophyll concentration during strongly stratified month of August. Phytoplankton growth earlier in the season would have depleted the nutrients in this region. Potentially upwelling along the slope, due to prevailing southerly wind, might have provided a source of nutrients (Siedlecki et al., 2008).

2. 3. 2. Mechanisms underlying the inter-annual chlorophyll variability

Over the 9-year time series, the magnitude of the enhanced chlorophyll in the fall-winter varied between 1.9 and 5.2 mg chl a m⁻³ (Figure. 2.9). One factor underlying the inter-annual variability was the presence of buoyant river plumes. In our data, the largest winter phytoplankton event occurred in 2006 and was associated with sustained high river discharge through the winter (Figure. 2.9). While precipitation of that year was normal, it was a warm winter and runoff was high as ice and snow formation was low. The 2006 river discharge event was observed by a Webb glider as a mid-shelf low salinity plume (as indicated by declines of 2 salinity units) in the upper mixed layer (Figure. 2.10b). The January 2006 winter plume was also evident as enhanced chlorophyll biomass in the SeaWiFS chlorophyll 4-day composite image from January 25th to 28th (Figure. 2.10a). The river plume is often transported out onto and south across the MAB under northwest wind conditions (Chant et al., 2008b). The plume can promote phytoplankton growth by stabilizing the upper water column and by transporting chlorophyll rich water from the estuary out onto the outer shelf offshore (Malone et al., 1983; Cahill et al., 2008). Additionally the river transports CDOM and non-pigmented particulate matter that can also lead to a 50-100% overestimate of chlorophyll (Harding et al., 2005). This suggests that years of high river discharge have the most biased satellite imagery. In spite of the potential satellite bias, the large river plume in 2006 contributed to the winter bloom as the river also transports extremely high concentrations of phytoplankton (Moline et al., 2008). While 2006 was the most sustained winter river discharge event, there were significant fall-winter discharge events in 1998, 2004, and 2005 that were also associated with winter blooms (Figure. 2.9); however, there were two

years (1999 to 2003) where no clear relationship between river discharge and winter bloom were found suggesting other factors are also important.

Another major factor influencing the inter-annual variability in the winter bloom magnitude was the frequency of storms. Storm-induced mixing lowers the irradiance available to the phytoplankton as cells are circulated deep in the water column. The role of the storms was difficult to study as storm periods are associated with heavy cloud cover. We measured storm frequency during the months of January and February using the NOAA moored buoy 44025 where a stormy day was defined as one when wind speeds exceeded 10 m s^{-1} . There was a significant inverse relationship between the percent of stormy days (storm) in the winter and maximum winter chlorophyll concentration (chl a) (Figure. 2.11a): $\text{chl a} = 4.34 - 0.05 \text{ storm}$ ($R^2=0.18$, $P=0.005$). In the winter, even small storms are able to induce significant mixing in the water column (Dickey et al., 2001; Glenn et al., 2008), which can increase overall light limitation of the phytoplankton populations. We hypothesize that the storm frequency and the river discharge are important to the winter phytoplankton as both impact the stability of the water column. Including winter river discharge in the estimation of the magnitude of the chlorophyll concentration improved the regression statistics ($\text{chl a} = 4.04 - 0.05 \text{ storm} + 0.000309 \text{ river}$ ($R^2=0.21\%$, $P=0.02$).

We performed a cluster analysis to explore the relationship between winter storm frequency, chlorophyll concentration and river discharge. Results from the ten years record clustered into two groups: one was 1998, 2000, 2003, 2004 and 2005; another was 1999, 2001, 2002, 2006 and 2007. As shown in Figure 2.11.a, these two clusters were

separated at a winter storm frequency 27%, which we hypothesize is the threshold where mixing is sustained to decrease overall seasonal winter phytoplankton concentrations.

The spring bloom occurred at the shelf-break/slope region. The spring bloom began in late March (mean start date was March 22nd) where we defined the start of the bloom as when the chlorophyll concentrations rise 5% above that year's annual median (Siegel et al., 2002). The initiation of the spring bloom was phased around 16 days after the onset of sea surface temperature warming on the MAB. This is consistent with the hypothesis that blooms begin as the water column stratifies and phytoplankton are maintained within the euphotic zone. Given this hypothesis, the timing of the spring bloom should be sensitive to weather conditions in the early spring that can precondition the shelf's stratification rate. Additionally, the timing of bloom can be important to the magnitude of the spring bloom. If a bloom starts late, it may miss the 'window of opportunity' with optimum mixing and light conditions, resulting in a reduced bloom magnitude (Henson et al., 2006). Using all available data there was not a significant relationship between the magnitude of the spring bloom and number of stormy days in early spring (February to March); however this was largely due to the spring 2003 which had a very high chlorophyll concentration despite moderate stormy conditions. Excluding 2003, there was a significant relationship ($\text{Chl } a = 3.62 - 0.0745 \text{ storm}$, $R^2=0.38$, $P=0.001$, Figure. 2.11b).

2. 4. Discussion

The 9-year of SeaWiFS chlorophyll dataset showed two distinct zones for phytoplankton activity on the MAB. The middle and outer shelf region was associated with the recurrent winter phytoplankton blooms. The outer shelf-break/slope region was

associated with the spring bloom. Although blooms in these two regions were separated in both space and time; however the magnitude of both blooms were both influenced by factors impacting water column stability.

Winter and spring phytoplankton blooms represent the major biological events in the MAB. The most recurrent and largest phytoplankton bloom occurs in winter, beginning in late fall and lasting through February. The winter bloom begins as the seasonal cooling erodes water column stratification, which results in the convective overturn of the water column. This process is accelerated by the passage of late fall storms (Glenn et al., 2008). The erosion of the stratification allows nutrient rich bottom waters to reach the surface alleviating nutrient limitation of phytoplankton within the euphotic zone. The spring bloom occurs on the outer shelf as seasonal warming begins to stabilize and stratify the water column. This is consistent with classical view advanced by Sverdrup (1953), and refined by Townsend et al. (1992) and Huisman et al. (1999), that phytoplankton blooms are initiated in nutrient replete waters when vertical mixing rates are slow so that phytoplankton photosynthetic rates are sufficient to support significant phytoplankton growth. Thus light regulation is central to both the winter and spring phytoplankton blooms on the MAB.

The winter blooms over the middle and outer shelf spanned the 20 to 60 m isobath as delineated by EOF mode 1. We hypothesize that this depth range reflected the zone where a significant fraction of the water column had sufficient light to support phytoplankton growth. We used the satellite chlorophyll and the Hydrolight radiative transfer model to estimate the depth of the 1% light level for EOF mode 1 region. In the EOF mode 1 region, the mean water depth was 41 m and the calculated mean 1% light

depth was close to 20 m; therefore 49% of the water column was above the 1% light levels (Table 1). This is significant as the winter blooms occur during the dimmest months of the year and incident light levels on the ocean surface are low. Even on the offshore side of the winter bloom at around 60 m a significant fraction of the water column resides above the 1% light level, which allows for significant photosynthesis (Falkowski and Raven, 2007). These calculations assume that the attenuation of light is only due to water and chlorophyll. In the MAB, especially when Hudson River water is present, there are other optical constituents (CDOM, detritus) that attenuate the light (Johnson et al., 2003). To assess the potential impact of the presence of Case II waters on the estimates of the 1% light depth, we combined the available optical measurements made in the Hudson River with Hydrolight. The turbidity of the Hudson River during the LaTTE experiment decreased as the water flowed offshore; therefore we calculated the impact for two scenarios. Scenario 1 was using data collected within the Hudson shelf valley where influence of Hudson River runoff was small. Scenario 2 was the offshore Hudson River, which represented turbid conditions within the Hudson River plume on the MAB. For these waters where river water was present, the depth 1% light level decreased to 10-20 meters depending on the rivers turbidity; however despite the increase in turbidity 25-50% of the water column in EOF mode 1 would remain above the 1% light level (Table 2.1). Thus in winter, phytoplankton appears to have sufficient light to grow when storm activity remains below the critical threshold of mixing.

The spring bloom occurred further offshore than the winter bloom and extended inshore of the MAB into shelf-break/slope area. Climatological temperature and salinity observations generally placed the foot of the front at the 80 m isobaths (Wright, 1976);

however, the front location can vary by as much as 20 km (Linder et al., 2004). Therefore, the shelf-break front can possibly affect the offshore extent of the winter bloom and generally coincides with offshore extent of the spring bloom. The shelf-break and slope area range from 200 to 681 m water depths and based upon the mean satellite measured chlorophyll the 1% light depth was 33 m. This euphotic zone represents 5-17% of water column. Therefore the phytoplankton blooms occur only after the solar radiation began to increase which increases the flux of light to the surface ocean and also helps stabilizing the water column by warming the surface water. This allows the cells to overcome chronic light-limitation in a deeply mixing water column (Sverdrup, 1953).

The temporal amplitude of the EOF analysis (Figure. 2.5) demonstrates the seasonal timing of chlorophyll blooms was consistent between years; however there was considerable inter-annual variability in the magnitude of the winter and spring blooms. The variability in the magnitude of the blooms was associated with factors that alter the water column stability. Winters with low storm activity were characterized by having large winter phytoplankton blooms. Additionally the middle and outer shelf can be significantly influenced by the Hudson River that can deliver large buoyant plumes (Castelao et al., 2008a). These buoyant plumes stabilize the water column and transports chlorophyll from estuaries onto the shelf (Moline et al., 2008). In contrast, the spring bloom requires the shelf-break/slope water to stratify before the bloom can occur. Once the system is stratified, the pycnocline on the MAB is extremely strong and is generally not disrupted until later autumn when wind mixing and surface cooling lead to convective overturn (Biscaye et al., 1994). Given this, the factors influencing the stratification rate are the key variable to predicting the shelf-break/slope phytoplankton bloom. In the work

of Lentz et al. (2003), they suggest that the direction, magnitude, and timing of spring wind stress events play an important role in inter-annual variations in stratification. For the unique year 2003, precipitation, river run-off, sea surface temperature and air temperature were not unusual and could not account for the high spring time chlorophyll concentration. The late winter 2003 were characterized by strong southwest winds, however, by early spring the winds shifted northeast. This resulted in predominately down-shelf and onshore transport. These northeast winds were not extremely strong in magnitude but they were sustained throughout the spring. Compare with other years, the 2003 spring had higher frequency of down-shore (53 days compared with the 11 year mean of 41 days) and towards-shore (48 days compared with the 11 year mean of 41 days) winds. Under such winds condition, there was convergence in the bottom waters at the shelf/slope, which can result in upwelling conditions that promote phytoplankton blooms (Siedlecki et al., 2008). Therefore, while regional pre-spring wind does impact the magnitude of the spring bloom, this relationship is not particularly robust as it can be overcome by local winds. The correlation between storminess and bloom magnitude was consistent with open ocean sites (Henson et al., 2006) where storms delay the stratification of the upper ocean.

Since the MAB hydrography strongly influence the spatial and temporal patterns in satellite chlorophyll, understanding these processes are critical as the shelf water of MAB is experiencing significant changes in its temperature, salinity (Mountain, 2003). Since the 1990s, the shelf water, which is the primary water mass in the MAB, has become warmer, fresher and more abundant than during 1977-1987. This has been correlated with transport of Scotian Shelf water and slope water and local atmospheric

heat flux (Mountain, 2003). These changes are likely to influence the stratification dynamics on the MAB. The freshening of the ocean can enhance vertical stratification that has been shown to be critical to the timing and magnitude of phytoplankton blooms (Ji et al., 2007). Additionally winter wind stress has increased in the last decade on the MAB and these changes have been associated with decadal declines in chlorophyll biomass in the fall and winter (Schofield et al., 2008). Given this, future work should focus on determining the critical thresholds between water stability and phytoplankton growth. While maximum chlorophyll concentration was affected by storm frequency and river plume are, other biological factors such as nutrient concentrations or grazing may also be important. This requires new data collected for sustained periods of time to complement satellite imagery. The use of gliders as observational platforms allowed for shelf waters to be sampled frequently over long periods of time. Therefore, we recommend gliders and satellite observations be focused during the transition season and provide the basis for evaluating the relationship between stratification/destratification and the blooms in the future.

Table 2. 1. Chlorophyll (mg m^{-3}) and light environment for the two regions defined by the EOF analysis in the MAB. For the shelf waters the 1% light depth was calculated using Hydrolight combined with optical data collected during the LaTTE experiment (Chant et al., 2008b, Moline et al., 2008).

Parameter	shelf (Zone 1)	shelf-break (Zone 2)
Mean Chl <u>a</u> (mg m^{-3})	1.7	0.7
Maximum Chl <u>a</u> (mg m^{-3})	4.9	2.1
Minimum Chl <u>a</u> (mg m^{-3})	0.6	0.2
Mean 1% Light depth (m)	20	33
Maximum 1% Light depth (m)	12	27
Minimum 1% Light depth (m)	36	55
Mean Water Depth (m)	41	200-681 ¹
Percent of water column above the 1% light (%)	49%	5-17%
Shelf valley ac-9 data 1% light depth (m)	20	
Offshore Hudson River ac-9 data 1% light depth (m)	10	

1: Much of Zone 2 occurs over the continental slope. Therefore we show the depths at the inner edge of the continental slope and the mean depth of Zone 2.

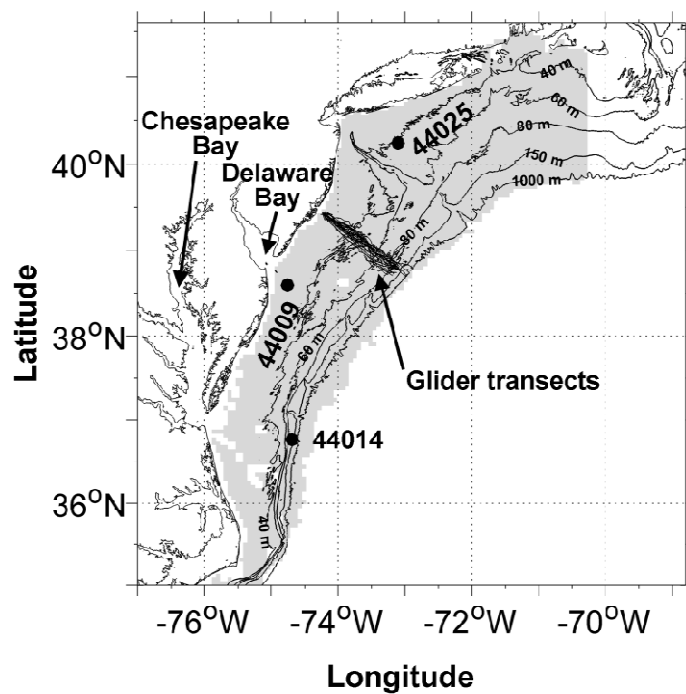


Figure 2. 1. Map showing study area, NDBC mooring stations, and glider track. Topographic contours shown are 40, 60, 80, 150, and 1000 m. Gray shaded area indicates location where SeaWiFS imagery was analyzed.

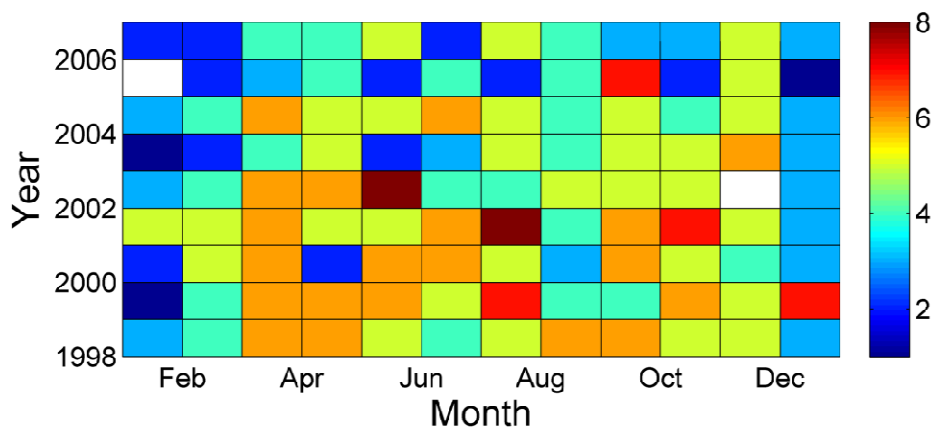


Figure 2. 2. Number of images used each in month for the entire time series of 4-day chlorophyll composites.

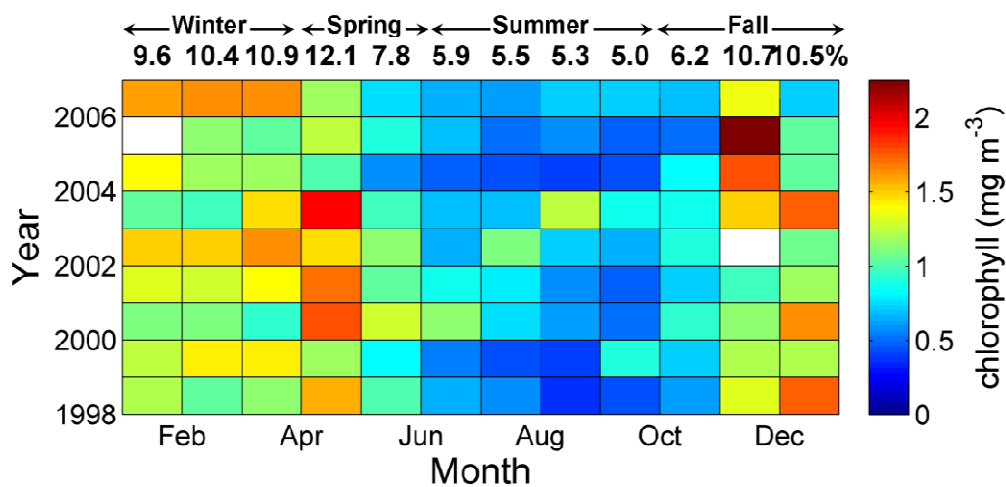


Figure 2. 3. Monthly mean chlorophyll (mg m^{-3}) from January 1998 to December 2006 for MAB (shaded gray area in Figure. 1). The numbers on the top indicate the relative percentage of annual mean chlorophyll for each month.

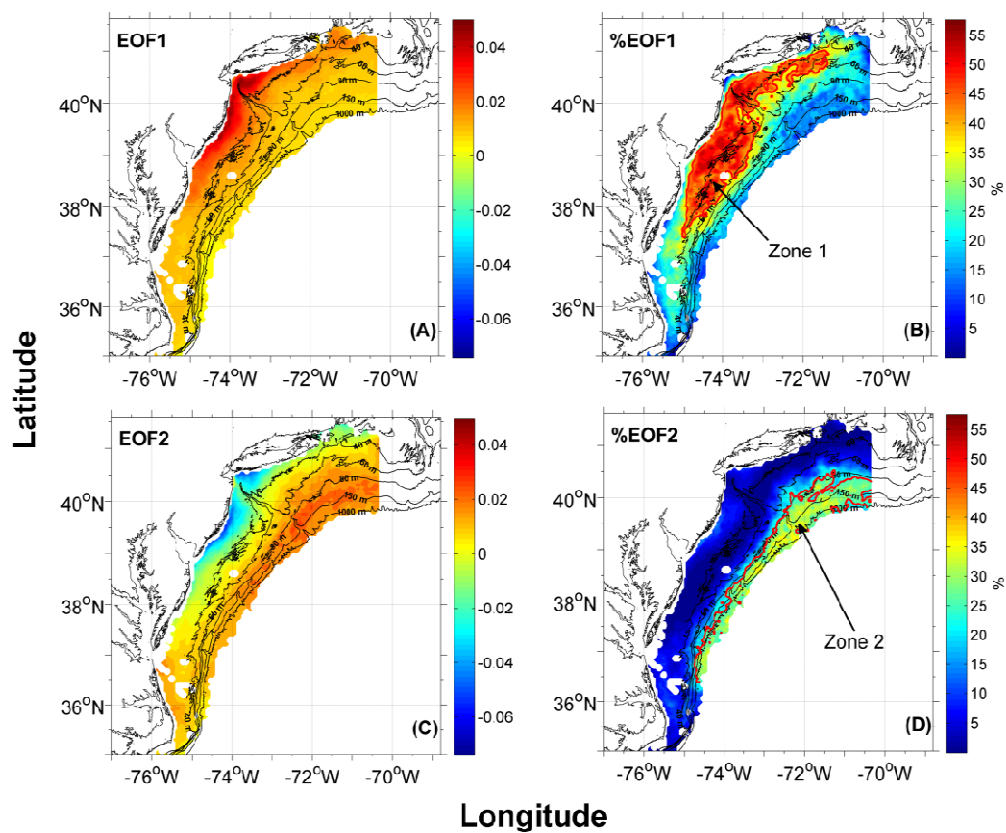


Figure 2. 4. The EOF modes for chlorophyll in MAB. Left panels are the first two EOF modes, right panels are percentage of the local variance explained by each mode.

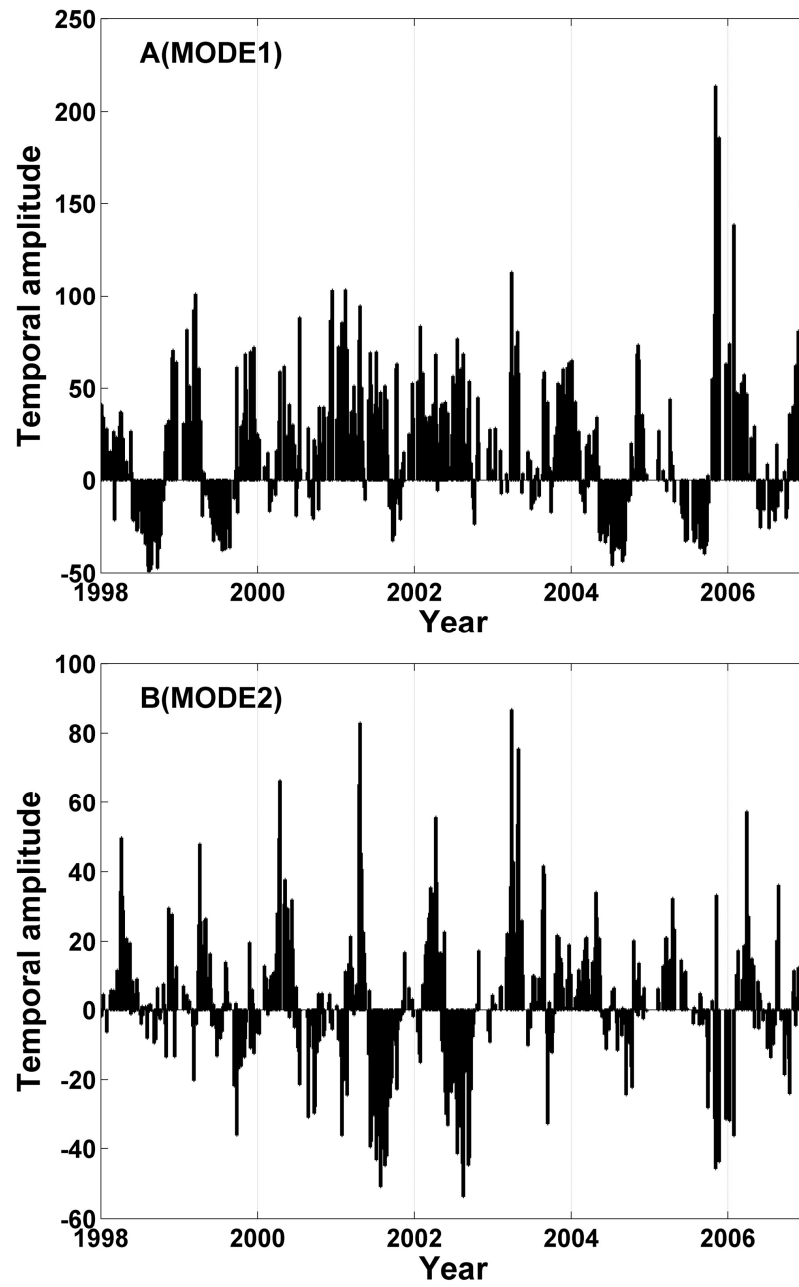


Figure 2. 5. Time series of the amplitude of the first two EOF modes.

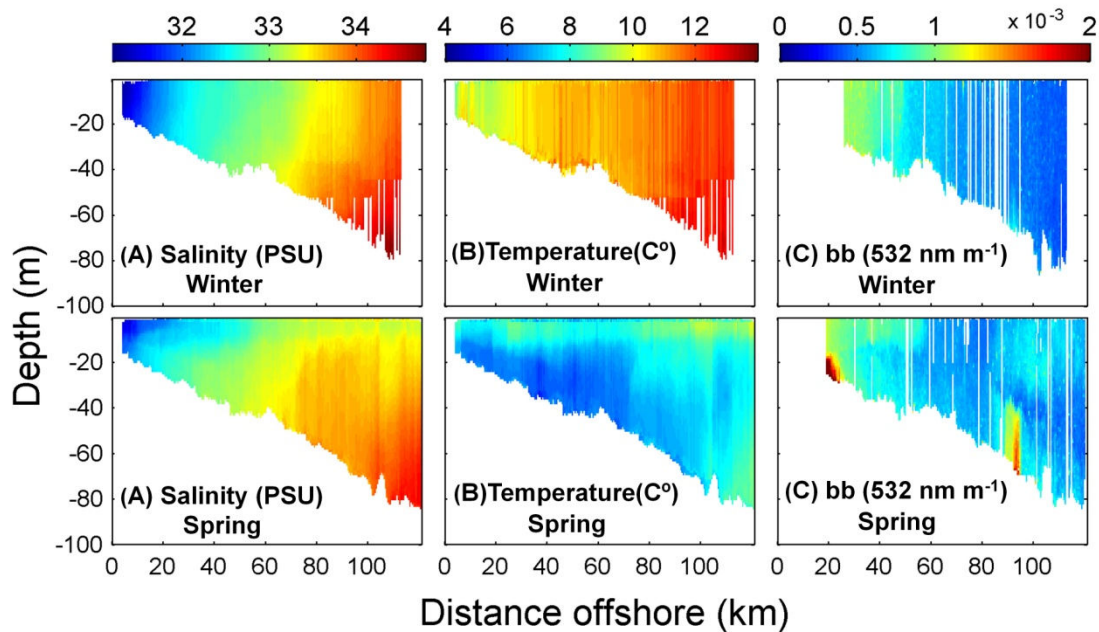


Figure 2. 6. Vertical sections of glider transect. Salinity (left), temperature (middle) and backscatter (right) collected along the Rutgers Glider Endurance line (See Figure. 1 for location; Schofield et al., 2007) during winter (top) and spring (bottom).

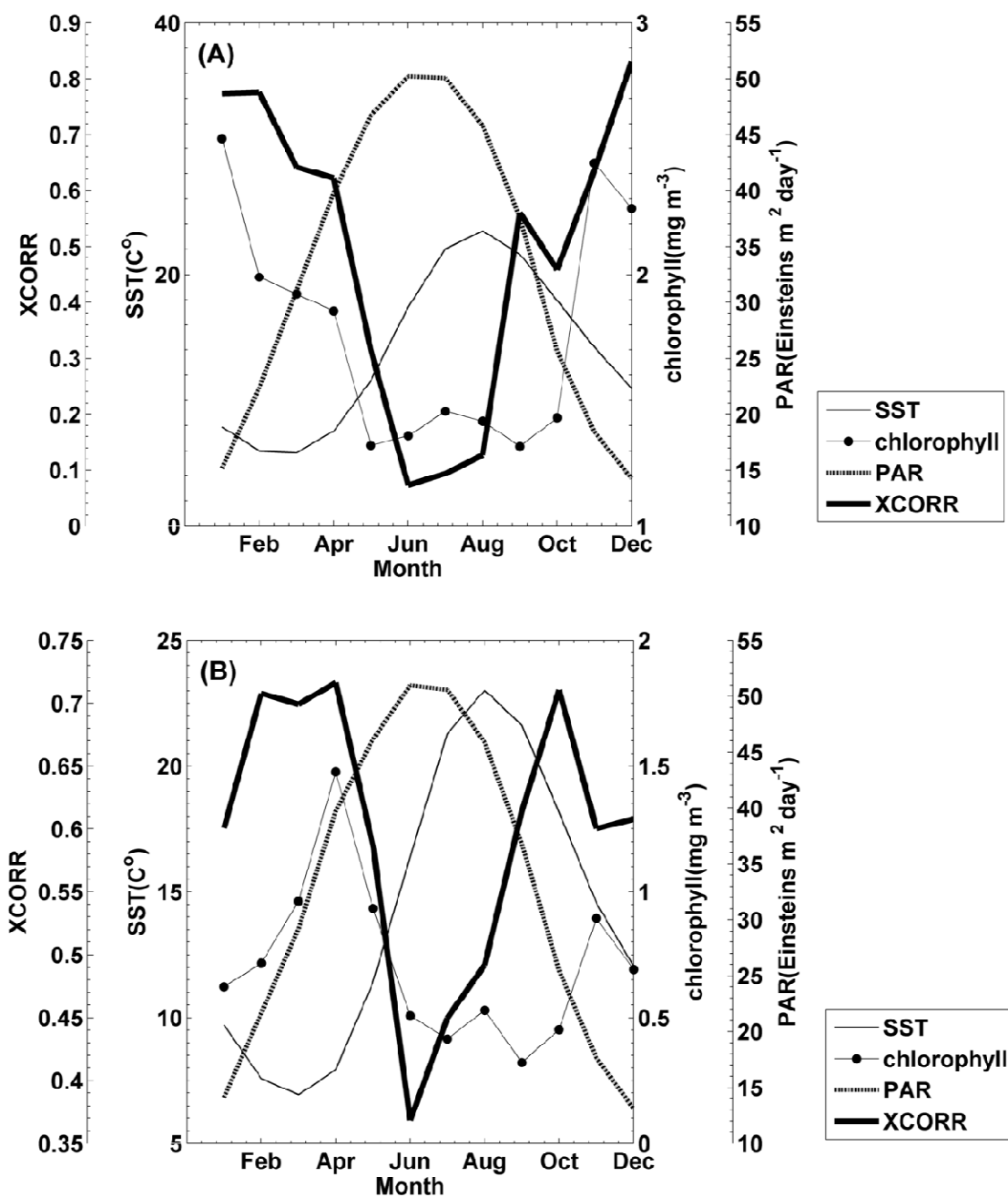


Figure 2. 7. Monthly climatology of SST (thin black line, °C), PAR (dash line, Einsteins m⁻² day⁻¹) and chlorophyll (thin line with dot, mg m⁻³) averaged over the two regions (Zone 1 and Zone 2 in Figure. 4) identified by the EOF analysis. Value averaged over

Zone 1 is shown on panel (A) together with correlation coefficient between cross-shelf wind and cross-shelf current (bold black line). Value averaged over Zone 2 is shown on panel (B), together with correlation coefficient between along-shelf wind and along-shelf current. In both panels, correlation analysis used wind observations from NDBC 44009 station, and HF radar currents along the cross-shelf line which is coincident with the glider endurance line (See Figure. 1 for location)

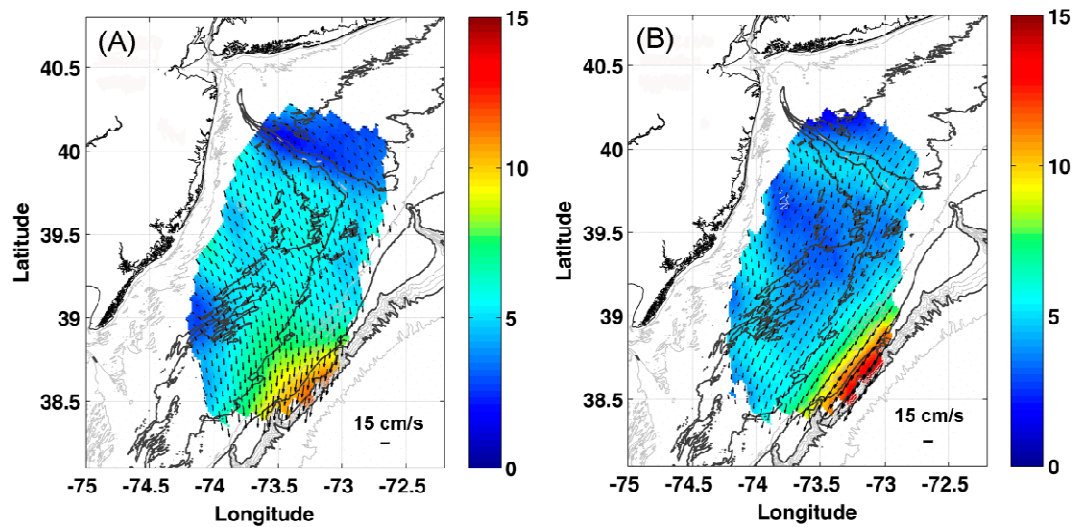


Figure 2. 8. Seasonal Surface current on the New Jersey Shelf (cm s^{-1}), vectors represent the current field and the color map is the magnitude of velocity: (A) Winter (December - February) (B) Spring (March - May).

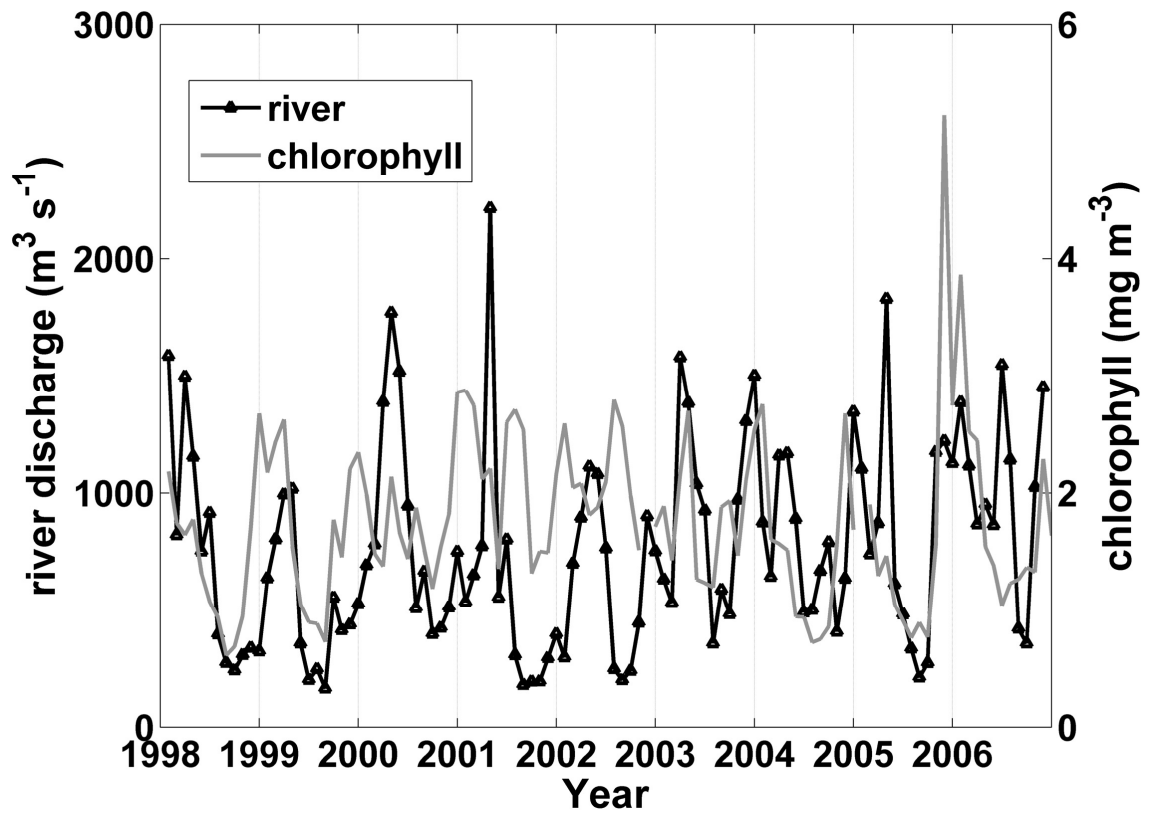


Figure 2. 9. Monthly and special averaged chlorophyll concentration (gray line) for area (Zone 1 in Figure. 4(B)) depicted by the EOF mode 1 (mg m^{-3}). The triangle marked black line represents the monthly mean river discharge in $\text{m}^3 \text{s}^{-1}$

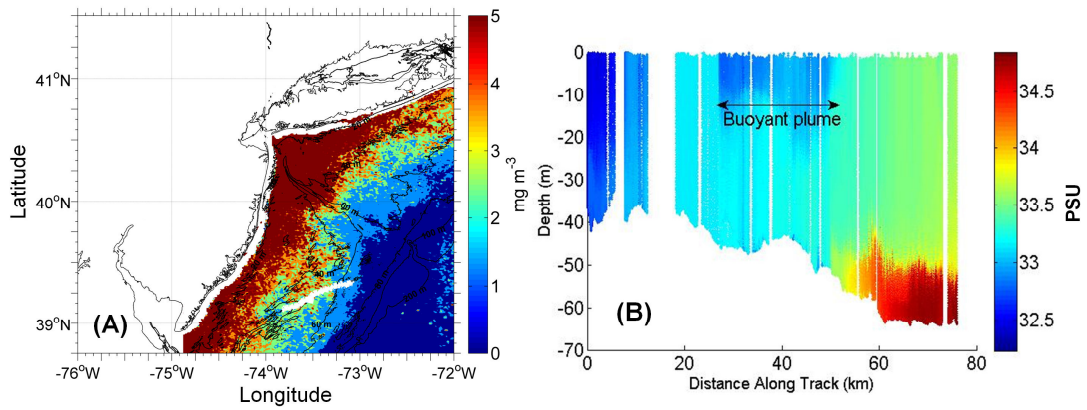


Figure 2. 10. (A) SeaWiFS chlorophyll 4-day composite image (January 25th to 28th, 2006). The white line on this panel indicates the location of the glider transect. (B) Salinity cross-section measured with a glider along the transect shown in panel (A). The glider measurement is from 2006 January 18th to 23rd.

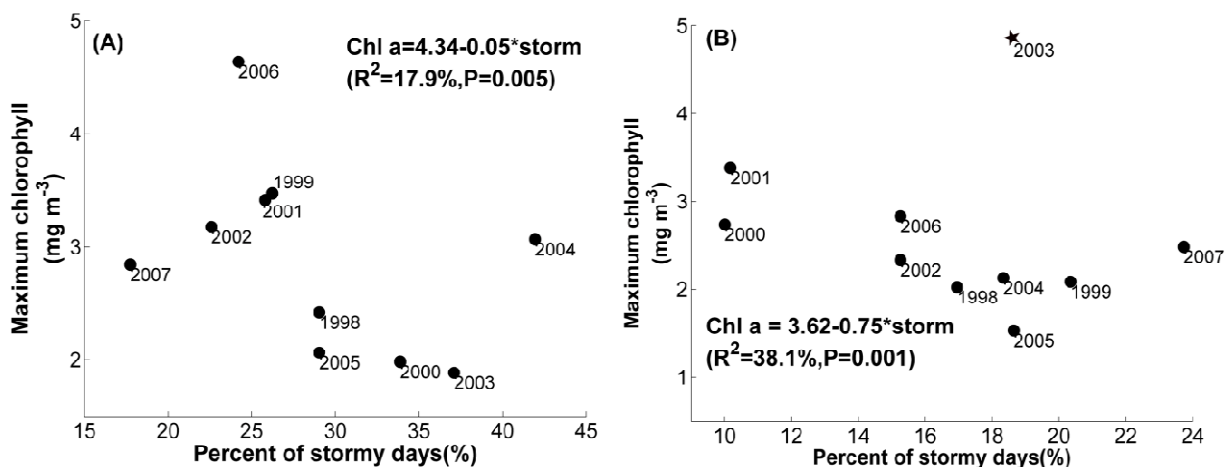


Figure 2. 11. (A) Percentage of stormy days against maximum SeaWiFS chlorophyll concentration (mg m^{-3}) in the area depicted by EOF mode 1, (B) Percentage of stormy days against maximum SeaWiFS chlorophyll concentration (mg m^{-3}) in area depicted by EOF mode 2. In panel (A), wind observations are from NDBC 44025 during Dec. to Jan., while in panel (B), winds are from NDBC 44014 during Feb. to Mar.; the star for 2003 means we consider it as an outlier.

CHAPTER 3. ROLE OF WIND IN REGULATING PHYTOPLANKTON BLOOMS ON THE MID-ATLANTIC BIGHT

3. 1. Introduction

The broad continental shelves of MAB have motivated numerous observational studies of the physical forcing of phytoplankton blooms. These studies have collected data with ships, satellites, moorings and gliders. These studies have documented the spatial and temporal variability in phytoplankton biomass in the MAB and have hypothesized about the key physical processes that underlie the observed variability. The 12-yr (1977-1988) NOAA NMFS Marine Resource Monitoring and Predication (MARMAP) survey of the Northeast of U.S. continental shelf found the highest phytoplankton concentrations during the winter-spring (O'Reilly and Zetlin, 1998). This was consistent with results from the Coastal Zone Color Scanner (CZCS) and Sea-viewing Wide Field of view Sensor (SeaWiFS) imagery that showed a fall-winter maximum of chlorophyll concentration in the middle and outer shelf waters and a spring maximum in the shelfbreak/ slope waters (Ryan et al., 1999; Yoder et al., 2001; Xu et al., 2011). Despite these large data sets, the observational studies did not have the spatial and temporal data required to link the environmental factors that underlie the phytoplankton dynamics. This has prompted the development of coupled ecosystem models to test hypotheses about the physical regulation of the MAB phytoplankton communities (Fennel et al., 2006).

Models describing phytoplankton dynamics must reconcile a phytoplankton's need for both light and nutrients, which are dependent on the overall mixing in the water column. The limitation of light to support phytoplankton growth builds on the Sverdrup (1953) "critical depth" model which predicts the initiation of phytoplankton blooms only after cells reside at a the critical depth where photosynthesis is larger than respiration allowing for the build-up of biomass. The maximum depth suitable for phytoplankton photosynthesis is most often defined as the depth where photosynthetic available radiation (PAR) is 1% of its surface value. While the absolute lower limit of light capable of supporting photosynthesis is still a subject of debate (Dubinsky and Schofield, 2010), estimates of the compensation depth irradiance based on Sverdrup's theory suggest it is relatively uniform throughout many regions of the ocean (Siegel et al., 2002). If light is present in sufficient quantities, the magnitude and duration of the bloom is then a complex function of mixing, nutrient availability (Tilman, 1982) and grazing pressure (Martin, 1965; Fasham et al., 1990; Turner and Tester, 1997; Gentleman et al., 2003). The flux of nutrients to the euphotic zone is determined by mixing across the nutricline, which can happen when the mixed layer depth (MLD) increases. These dynamics in the MLD thus has been demonstrated to be a key factor in determining phytoplankton abundance (Falkowski and Raven, 2007); however while vertical mixing in the upper-ocean boundary layer can increase productivity in the surface waters through enhanced nutrient supply from deep waters it can also decrease productivity due to mixing phytoplankton below the critical depth and leading to light limitation (Dutkiewicz et al., 2001). To parameterize the relative roles of mixing and light availability the ratio of Z_{mld} (mixing layer depth) to Z_{eu} (euphotic depth) has been used to describe the regulating

primary production (Irigoiien and Castel, 1997; Huisman, 1999); however, this ratio only reflects the relationship between light attenuation coefficient and MLD. Therefore, the

ratio of integral of light in the euphotic zone and MLD ($\int_{-Z_{eu}}^0 I(z) * dz / Z_{mld}$) might be a preferred value to compare the balance between light limitation and nutrient limitation.

For this study, we use time series of satellite chlorophyll and 3-D biophysical model simulations to investigate the relative importance of mixing rates and light availability for phytoplankton populations in the MAB

3. 2. Methods

3. 2. 1. The Biogeochemical Model

In this study we used the Regional Ocean Modeling System (ROMS, <http://www.myroms.org>) (Haidvogel and Beckmann, 1999; Wilkin et al., 2005) which was configured to the continental shelf of the Middle Atlantic Bight (MAB) (The model domain is shown in Figure. 3.1). The model has a horizontal grid resolution of approximately 5 km, and uses 36 vertical layers in a terrain-following s-coordinate system. The biogeochemical model was developed and described in Fennel et al. (2006). The model here assumes nitrogen is the major limiting nutrient, which is a reasonable assumption as nutrient budgets indicate nitrogen limitation is frequently observed in the MAB (Ryther and Dunstan, 1971; Sharp and Church, 1981). Also nitrogen availability in the MAB is found the key nutrient to accurately simulating primary production (Fennel et al., 2006). The basic structure of this model follows a classical Fasham model (Fasham et al., 1990) and is constructed using seven state variables: phytoplankton, zooplankton, nitrate, ammonium, small and large detritus, and chlorophyll. The time rate change of

phytoplankton is influenced by the growth rate of phytoplankton, grazing by zooplankton, mortality, aggregation of phytoplankton to small and large detritus, and vertical sinking of the aggregates. This model drives phytoplankton growth (μ) through variations in temperature (T) (Eppley, 1972), incident light intensity (I) (Evans and Parslow, 1985), and the availability of nutrients (Parker, 1993), following

$$\mu = \mu_{\max} \cdot f(I) \cdot (L_{NO_3} + L_{NH_4}) \quad (1)$$

μ_{\max} is the maximum growth rate which depends on temperature. I is the photosynthetically available radiation and decreases with water depth due to absorption by seawater (assumed constant) and the time and spatially varying chlorophyll computed by the model.

$$I = I(z) = I_0 \cdot par \cdot \exp\left\{-z(K_w + K_{chl} \int_z^0 Chl(\zeta) d\zeta)\right\} \quad (2)$$

where I_0 is the surface incoming light and is the shortwave radiation flux from NCEP reanalysis data, par is the fraction of light that is available for photosynthesis and equals 0.43. K_w and K_{chl} are the light attenuation coefficients for water and chlorophyll, and are set to 0.04 m⁻¹ and 0.025 (mg Chl)⁻¹ m⁻² respectively (Fennel et al., 2006). The $f(I)$ represents the photosynthesis-light (P-I) relationship. The parameter α is the initial slope of the P-I curve. The terms L_{NO_3} and L_{NH_4} represents the nutrients limitation.

$$f(I) = \frac{\alpha I}{\sqrt{\mu_{\max}^2 + \alpha^2 I^2}}, \quad (3)$$

$$L_{NO3} = \frac{NO3}{K_{NO3} + NO3} \cdot \frac{1}{1 + NH4/K_{NH4}}, \quad (4)$$

$$L_{NH4} = \frac{NH4}{K_{NH4} + NH4}. \quad (5)$$

The rate of grazing by zooplankton is represented by a Holling type s-shaped curve (Gentleman et al., 2003). The mortality loss term has linear relationship with phytoplankton. The aggregation rate is assumed to scale with the square of small particle abundance for more details see Fennel et al., 2006. The model was driven by atmospheric forcing provided by the North American Regional Reanalysis (NARR) from the National Centers for Environmental Prediction (NCEP). We used a 3-hourly re-analysis of surface air temperature, pressure, relative humidity, 10-m vector winds, precipitation, downward long-wave radiation, and net shortwave radiation to specify the surface fluxes of momentum and buoyancy using bulk formulae (Fairall et al., 2003). In the open boundary, we specified temperature, salinity, nitrate (NO₃). Because the focus of this study is the influence of wind forcing on phytoplankton dynamics, the open boundary inputs are specified by the climatology input based on the Fennel ROMS model simulation of the Northeast North American (NENA) shelf (Fennel et al., 2006). We included the inputs of seven rivers (Hudson, Connecticut, Delaware, Susquehanna, Potomac, Choptank, and James River) on the boundary. River outflow was provided by the daily mean outflow from the United States Geological Survey (USGS) gauges (available online at <http://waterdata.usgs.gov/nwis/>). The riverine inputs of temperature, salinity, dissolved and particulate biological constituent concentrations were derived from the total nitrogen in the nitrate pool follow Howarth et al., (1996). Here the concentrations were assumed

time invariant and inputs were multiplied by the freshwater discharge to give total nutrient inputs for each river. The model is initialized with model output in this domain described in Hofmann et al. (2011). The 4-yr (2004-2008) duration simulations were conducted with the first year used as a spin-up period. Results presented here are from the analysis of the final three-years of simulation.

3. 2. 2. Glider Observations

Webb Slocum gliders data was collected as part of local and regional glider time series in the MAB (Schofield et al., 2010, Figure. 3.1). The time series is not formally founded and thus is not a complete monthly time series; however the time series is a large data base providing vertical profiles of temperature and salinity. A smaller subset of chlorophyll data was available, however it should be noted that not every glider is equipped with a fluorometer. The data base used for this study spans from 2006 and 2008. During the periods, there are three missions (June 2006, July 2006, and July 2007) along Rutgers University Glider Endurance Line (RUEL) and three missions (March 2007, April 2007, and March 2008) along Multidisciplinary University Research Initiative Line (MURI). For the RUEL transect, it takes approximately 5-10 days to be completed, while for the MURI transect, it takes 12- 25 days to be completed. The majority of the glider observations provide data for spring and summer time. These efforts provide over 8257 vertical profiles with temperature, salinity and chlorophyll data that were included in this study. For each profile, we calculated light (I) based on equation (2). All gliders are equipped with a Sea-Bird conductivity-temperature-depth (CTD) sensor, which was used to calculate the MLD based on the measurement of temperature and salinity. The MLD was defined as the depth lower 0.125 kgm^{-3} than potential water density at the surface.

3. 3. Result

3. 3. 1. Model Simulation and Observations of MAB phytoplankton

We have focused our analysis of the seasonal variability in phytoplankton in Zone 1 and Zone 2 as identified in Figure 2.4. Time series of the 4-day average chlorophyll for both zones are shown in Figure 3.2. Generally, the chlorophyll in Zone 1 showed a persistent phytoplankton bloom in the late fall and winter that typically lasted several weeks despite the solar illumination being lowest during this time of year. The timing of this bloom has been related to the seasonal destratification of the MAB, which replenishes nutrients to the surface waters. The magnitude of bloom has been related to the overall wind-induced mixing with the frequency of winter storms determining the overall seasonal light-limitation of the phytoplankton (Xu et al., 2011). In contrast, the phytoplankton blooms in Zone 2 occur in the spring and are associated with the onset of stratification in the deeper waters of the outer shelf (Figure. 3.2b). The spring bloom is shorter and has lower concentrations of chlorophyll than the fall-winter bloom. These seasonal cycles of chlorophyll are consistent with the in situ MARMAP data (Yoder et al., 2001, shown in Figure. 6), that show peak chlorophyll values occur during fall-winter in middle and outer shelf water and a distinct spring maximum in shelf-break slope waters (Yoder et al., 2001).

The satellite measured chlorophyll dynamics were successfully reproduced by the biological model (Figure. 3.3). The simulated sea surface temperature was also in the standard deviation range when compare with the climatology measurement from NDBC

buoy 44009 (Figure. 3.4c). The simulated chlorophyll in Zone 1 increased in late fall and lasted through the winter. The correlation found between simulated chlorophyll and SeaWiFS chlorophyll was 0.48 ($p < 0.001$, Figure. 3.4a) which was mainly due to the winter bloom. The bloom showed a bimodal peak with lower concentrations found during the darkest periods of winter which was not readily evident in the satellite data that perhaps reflect the relatively low availability of ocean color images during the cloudy winter (Xu et al., 2011). The model also successfully simulated the timing and magnitude of spring bloom in Zone 2, which could explain ~74% of the log-transformed variance of the observed chlorophyll ($p < 0.001$, Figure. 3.4b).

The model overestimated observed chlorophyll and likely reflects the poor prediction of zooplankton grazing for the following reasons. During the SEEP II experiments in this area (Flagg et al., 1994), zooplankton concentrations ranged from 0.4 to 28.6 mmol N m⁻³. Our modeled zooplankton concentrations varied from 0 to 2 mmol N m⁻³, which is within the range observed during SEEP II (Flagg et al., 1994) but at the lower end of the observations. If grazing pressures were too low, then major factor regulating the termination of the spring bloom in the model would be the depletion of nutrients. This would result in the modeled spring bloom lasting longer than the satellite observations which would be impacted by the zooplankton grazing. The spring bloom based on the 4-day average SeaWiFS data typically lasted 12-20 days over the ten-year data set (Figure. 3.2b). The spring bloom in the model simulations typically lasted for 30-40 days (Figure. 3.2b), which would be consistent with the model that underestimating grazing pressure.

3. 3. 2. Environmental regulation of phytoplankton

Accepting that the model describes the general variability observed for chlorophyll, we used the model simulations to analyze the physical factors regulating phytoplankton biomass on the MAB. Time series of the modeled chlorophyll and key environmental variables (temperature, upper mixed layer, light, nutrients, and zooplankton) for both zones are shown in Figure. 3.5 and Figure. 3.6. In Zone 1(Figure. 3.5), water column cooling resulted in destratification, which was reflected as an increase in the upper mixed layer depth from 10 meters at the beginning of October to 30 meters deep at the end of February. The deepening of the upper mixed layer depth was associated with an increase of nitrate within the euphotic zone. Nitrate exhibited considerable variability within the upper 20 m showing that convective overturn and entrainment processes were effective increasing nutrients in surface waters. Nitrate within the mixed layer was consumed rapidly by phytoplankton from December through March. Phytoplankton growth was significant even during the dim winter months as >50% of the water column was above the 1% light level depth. Phytoplankton biomass remained high until the upper mixed layer depth began to shallow and nitrate was rapidly depleted and grazing pressure increased. After surface nitrate was depleted, a significant subsurface phytoplankton peak was maintained at the nutricline throughout the year.

In contrast, phytoplankton blooms in Zone 2 were found primarily in the spring with a smaller secondary bloom in the fall when stratification began to weaken (Figure. 3.6). No winter phytoplankton bloom was observed as the upper mixed layer was deep and the majority of the water column was below the 1% light level (Xu et al., 2011). The spring phytoplankton bloom formed in March every year during the simulation as the upper mixed layer depth decreased and nitrate concentrations were high. The nutrients

were consumed in several weeks and nutrient depletion resulted in the termination of the bloom. As observed in Zone 1, a subsurface phytoplankton bloom formed, however the nutricline was deep and the subsurface concentrations of chlorophyll were less than half then observed on the inner continental shelf.

The relative limitation of phytoplankton by light and nutrients is tightly coupled to the depth of the upper mixed layer as is illustrated in Figure 3.7. The threshold for light limitation is described as equation (3). The threshold for nutrient limitation in the model is calculated as equation (4) and equation (5). Value of 1 indicates no limitation. During winter months, when the upper mixed layer is deep, the majority of the phytoplankton in the water column are light limited (<0.8 , Figure. 3.7a), however nutrient limitation is low (>0.8 , Figure. 3.7b). As solar illumination increases in spring, the mixed layer depth shallows and light limitation is decreased; however the entrainment of nutrients to surface waters is decreased and nitrate limitation begins to increase as the phytoplankton grow rapidly. In the euphotic zone, where there is sufficient light for photosynthesis, the reduction of CO_2 to organic carbon fuels the rate of cell doubling and population growth. Thus, the availability light drives the flux of carbon, and other elements, into cells and thereby determines the rate at which nutrients are utilized by photoautotroph for growth (Dubinsky and Schofield, 2010).

To test the role of mixing in regulating phytoplankton bloom dynamics we conducted a series of model simulations. Five different wind cases were applied: no wind forcing, wind stress increased to 25% of normal wind, normal wind, increased to 125% of normal wind and increased to 150% of normal wind. The responses of spatial mean chlorophyll in Zone 1 under different scale of wind were shown in Figure 3.8. The

relationship between wind forcing and chlorophyll varies by season. Except for winter, there is an increase of chlorophyll concentration with increase wind forcing. The reason for this is because too much mixing in winter would unstable water column and increase light limitation. In contrast, for other seasons, wind mixing is needed to maintain nutrient supply. So, chlorophyll increases with enhanced wind. For all the season, the chlorophyll change dramatically from no wind to normal wind condition, however these trends turn to mild after the wind force change from normal wind to 1.5 of normal wind. So here we compared the models driven by measured wind (as above) to hypothetical simulations where no wind was applied to the ocean. Comparisons of the simulations for both Zone 1 and Zone 2 are shown in Figure 3.9. In Zone 1, the “no wind” condition resulted in fall blooms later in the season, which reflects the importance of wind mixing combined with seasonal cooling to drive the convective overturn on the MAB. The “no wind” condition does not show convective overturn and replenishment of nutrients to the surface waters until several weeks later in the season (Figure. 3.10d). The mid-winter depression in the winter bloom is not present in the “no wind” simulation. The magnitude and timing of the winter bloom is strongly tied to storms, which induce mixing during the dim winter months leading to increased light limitation of the phytoplankton (Xu et al., 2011); therefore the “no wind” condition diminishes mixing and light limitation and allows for larger winter blooms. The decline in the winter light limitation is also visible in the “no wind” plot (Figure. 3.11a, black line). Finally, as the spring transition begins and the water column begins to stratify due to increased radiant heating, the phytoplankton in the “no wind” experiment showed a more rapid biomass decrease reflecting an earlier onset of nutrient limitation (Figure. 3.11a). For Zone 2, the “no wind” condition resulted in an

earlier spring bloom (Figure. 3.9b) reflecting the earlier onset of stratification of the offshore waters. This is consistent with satellite analyses that suggested pre-spring storms strongly influenced the timing and magnitude of the spring bloom in the MAB (Xu et al., 2011). The other major differences in Zone 2, is that the spring phytoplankton activities were higher under the normal windy conditions (Figure. 3.9b), which alleviated the early onset of nutrient limitation as the MLD became shallower (Figure. 3.11b). Finally the fall bloom observed in Zone 2 was not present (Figure. 3.9b), as the convective overturn on the MAB was delayed and cells were nutrient limited (Figure. 3.11b).

3. 3. 3. Light, upper mixed layer depth, and chlorophyll

There is an inverse relationship between the MLD and the average light levels within the MLD (Figure. 3.12). This relationship varies between Zone 1 and Zone 2, with offshore waters having a higher mean irradiance in the MLD. This reflects that the waters on the continental shelf are more turbid due to the enhanced attenuation of light by chlorophyll, colored dissolved organic matter and non-algal particles found in the shelf waters of the MAB (Schofield et al., 2004). While peak phytoplankton biomass ($>4 \text{ mg m}^{-3}$) is found over a 5-fold range of MLDs, there is a narrow range (50%) of mean irradiances associated with peak phytoplankton concentrations (Figure. 3.9). Peak chlorophyll values in Zone 1 were associated with lower mean light intensities compared to Zone 2. In order to parameterize both the MLD and light critical threshold of light to induce phytoplankton blooms we calculated modified mixing-light value (I') as the ratio of integral of light (I) in the euphotic zone (Z_{eu}) divided by the MLD (Z_{mld}) as

$$I' = \int_{-Z_{eu}}^0 I(z) * dz / Z_{mld} \quad (6)$$

The I' term incorporates both the incident light and the mixing environment through the depth of the MLD. The MLD also contains information on the probability of nutrient availability. We assessed if there is a critical I' value associated with both the observed and simulated chlorophyll maximum ($I'_{chl\ max}$). The I' values derived from the model were integrated into 20 $W\ m^{-2}$ bins for Zone 1 and Zone 2 (Figure. 3.13). There is an increase in chlorophyll with increasing I' up until 60 and 160 $W\ m^{-2}$ ($I'_{chl\ max}$) for Zones 1 and Zone 2 respectively. Under these conditions, deeply mixed layers limited phytoplankton growth as overall light levels were low. For the waters of Zone 1 with shallow water depths, the mixed layer only need to decrease slightly to ensure that the majority of the water column is within the euphotic zone and phytoplankton have sufficient light to grow. In Zone 2, the deeper water depths require the MLD to decrease significantly in order to overcome light limitation. After this threshold has been reached, increasing I' is associated with declining chlorophyll. Here cells are maintained under high light but a shallow MLD does not allow for replenishment of the nutrients from depth. These chlorophyll and I' relationships were compared to chlorophyll data measured with Slocum gliders outfitted with fluorometers (Figure. 3.13, black line with dots). Despite that the glider data set is smaller and does not include many transects during the winter months, the relationship between I' and chlorophyll is similar showing an increase at low I' values to a value of 50 $W\ m^{-2}$ and then decreasing values as I' increases. The glider chlorophyll values are lower than model estimates which is not surprising as the data set does not include many transects during the winter bloom. Calculations of I' for the “no wind” simulation show similar patterns except that it takes

a high magnitude of I' to reach the peak chlorophyll values for Zone 2 (Figure. 3.16 plus line).

Is $I'_{chl\ max}$ predictable? Spatial maps of $I'_{chl\ max}$ associated with the chlorophyll maximum for the MAB are shown in Figure 3.14. Generally, $I'_{chl\ max}$ is low and relatively constant on the continental shelf and increases in magnitude out over the continental slope and deep sea. The one shallow water exception was associated with the Hudson River plume, which is extremely turbid and mixing rates in the buoyant plume water must be high enough to overcome chronic light limitation for phytoplankton bloom (Schofield et al., 2011). Excluding this river zone, the relationship between $I'_{chl\ max}$ and bottom depth were robust (Figure. 3.15). Bottom depth could explain 70% of the variability in $I'_{chl\ max}$ ($p < 0.001$).

3. 4. Discussion

The late fall-winter bloom is the most recurrent and largest phytoplankton bloom in the MAB (Ryan et al., 1999, 2001; Yoder et al., 2001; Xu et al., 2011). The fall-winter bloom is fueled by the replenishment of nutrients to the euphotic zone once the summer thermal stratification has been disrupted. This thermal stratification is dramatic (summer thermoclines on the MAB exhibit a temperature gradient of over 15° Celsius in only 5 meters water depth, cf. Castelao et al., 2010) and this stratification deprives the surface phytoplankton of macro and micronutrients throughout the late spring, summer and early autumn. Observational studies have documented there is a great deal of inter-annual variability in the timing of the late fall-winter bloom (Yoder et al., 2001). The variability in the timing of the bloom has been related to the timing of destratification, which is

driven by seasonal cooling of the surface waters and the passage of large storms that induce wind mixing (Beardsley et al., 1985; Lentz et al., 2003; Glenn et al., 2008). The magnitude of the fall winter bloom is thought to be regulated by factors that stabilize the water column (Xu et al., 2011). In the MAB, these processes include the frequency of winter storms and the presence of low salinity buoyant plumes (Xu et al., 2011). While the observational data is compelling it has been insufficient to confirm the hypothesized forcing of the late fall-winter phytoplankton bloom.

To test the hypothesized physical forcing of the MAB phytoplankton we utilized the physical-biological ROMS model to conduct a series of simulations where we varied the physical forcing and analyzed the source and sinks of the phytoplankton. The model which used realistic forcing was able to simulate the timing and spatial extent of the phytoplankton dynamics observed in SeaWiFS data. The model did a quantitatively good job of predicting the winter bloom; however the model had a more difficult time in reproducing the magnitude of the spring bloom. For the spring bloom region, there are large horizontal and vertical gradients in water properties and are associated with the shelf-break front, a feature susceptible to nonlinear instabilities and strong interactions with Gulf Stream warm-core rings (Gawarkiewicz et al., 2001; 2004). As a result, this region has complicated physical background that the mixing by wind cannot really be isolated. The discrepancy for the spring bloom likely reflected both by underestimated in chlorophyll by satellite-derived chlorophyll in this region (Fennel et al., 2006) and underestimated zooplankton grazing (Flagg et al., 1994). For the late fall-winter bloom, our numerical experiments explicitly demonstrated the role of wind mixing in winter phytoplankton dynamics when all the other forcing factors were held constant. For the

initiation of the late fall-winter bloom the no wind mixing simulation demonstrated that wind was a secondary factor; therefore seasonal cooling and the corresponding convective overturn on the MAB is the dominant feature initiating the phytoplankton bloom. This is consistent with observations that tropical storms on the MAB can only induce water column turnover if the summer thermocline had been previously weakened by seasonal cooling (Glenn et al., 2008). After destratification, the frequency of high wind regulates the size of the phytoplankton bloom. Strong winds result in high mixing rates or less solar radiation because of cloudy weather, which results in the light limitation of the phytoplankton (Xu et al., 2011), which is confirmed by the model as an increased wind forcing resulted in smaller phytoplankton blooms.

Wind forcing also has a significant role on the timing and magnitude of the offshore spring bloom. Observational efforts have related the size and timing of the spring phytoplankton to the amount of wind mixing present in the late winter (Xu et al., 2011). Wind mixing in the late winter delays the thermal stratification of the MAB, which influences the spring bloom as cells require water column stabilization to overcome light limitation. During the no wind simulation, the spring bloom was dominated by a single event that occurred earlier in the season compared to normal wind conditions. This bloom was short lived as the cells rapidly consumed available nutrients. In contrast, the model simulation that used natural wind forcing resulted in a spring bloom that lasted longer throughout the season compared to the no wind condition as wind mixing replenished the supply of nutrients and enhanced the overall amount of chlorophyll on the MAB. The SeaWiFS observed bloom in the shelf-break front region commenced in late March and lasted up to late April. In our simulated case with wind,

the spring bloom in the shelf-break front region initiated in early March and lasted up to early April. It looks like that although the model simulated spring bloom start a little bit earlier under normal wind condition, it can better capture the both spring and fall bloom in this region compare with no wind forcing condition.

Is there a relatively predictable light condition that promotes a maximum chlorophyll concentration? Photosynthetic activity is confined to the euphotic zone, which is nominally defined as the depth where the light levels are 1% of the surface light intensity. The depth of the euphotic zone is poor at predicting the initiation of phytoplankton blooms as any mixing to depth limits phytoplankton biomass accumulation in the upper mixed layer. This is due to the high respiratory costs to build cells (Falkowski and Raven, 2007). This discrepancy is accounted by Sverdrup's (1953) "critical depth" for bloom initiation (Smetacek and Passow, 1990; Obata et al., 1996). This framework has been highly effective for the open ocean where the compensation depth for phytoplankton growth appears to be relatively constant (Siegel et al., 2002). In MAB, the light regime is tied closely to mixing regime as light is rapidly attenuated by high phytoplankton biomass and significant inputs from buoyant turbid plumes (Cahill et al., 2008; Castaleo et al., 2008). As mixing determines not only the light but also the nutrient availability, there is need to parameterize the relative impacts of both. To parameterize the relative tradeoffs of mixing and light availability, the ratio of Z_{mld} to Z_{eu} has been used to describe the regulating primary production (Irigoiien and Castel, 1997; Huisman, 1999); however, this ratio only reflects the relationship between light attenuation coefficients and MLD. We suggest that it is more appropriate to use I' which is the ratio of integral of light in the euphotic zone and MLD to compare the balance

between light limitation and nutrient limitation. When I' is low, phytoplankton is light-limited due to low surface irradiance and deep mixed layer. The variability shows a single peak in both offshore and nearshore conditions. At high values of I' , the mixed layer is shallow, coincident with the seasonal increase in solar illumination, which allowed the photosynthetic activity to consume the available nutrients. This in turn results in low biomass. We used the model to define this integral and then assess when it results in the maximum chlorophyll biomass ($I'_{chl\ max}$). Model simulations suggest that on MAB, $I'_{chl\ max}$ varied by a factor of three and were spatially variable. The spatial variability was positively correlated with water depth, suggesting that this term can be parameterized.

Our results based on numerical simulation and glider observations confirm the SeaWiFS observation of seasonal phytoplankton bloom in the MAB. The modified light values are used to describe the balance between light and nutrients limitation which act to influence the timing and magnitude of bloom. Sensitivity study of no wind forcing simulation proves that the mixing plays a significant role in regulating the nutrient and light field and thus influences the phytoplankton dynamics.

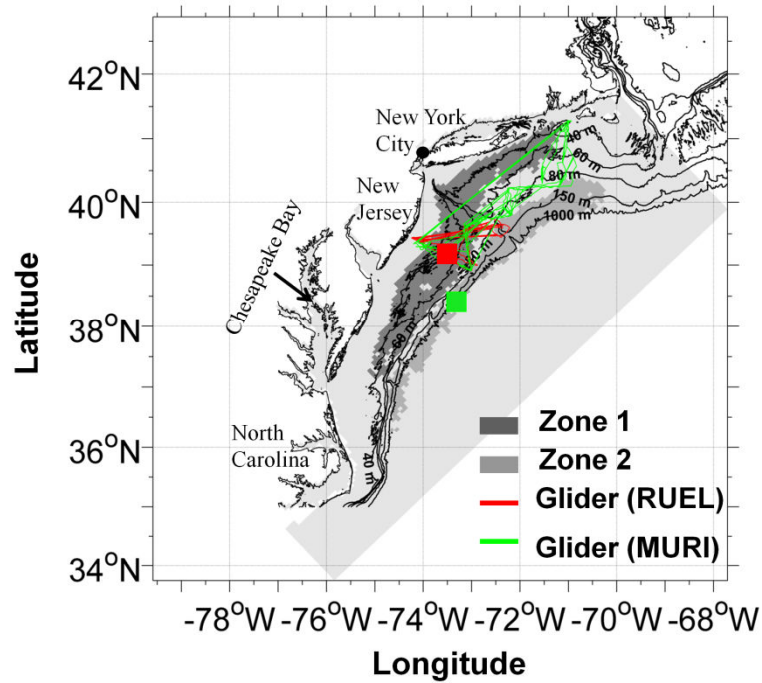


Figure 3. 1. Model domain (light grey). Dark grey and grey highlight the Zone 1 and Zone 2 region identified by Xu et al. (2011). Red and green lines show the glider transects. Red and green square symbols represent the grid point used for calculation in Zone 1 and Zone 2. The black lines with number show the bathymetry.

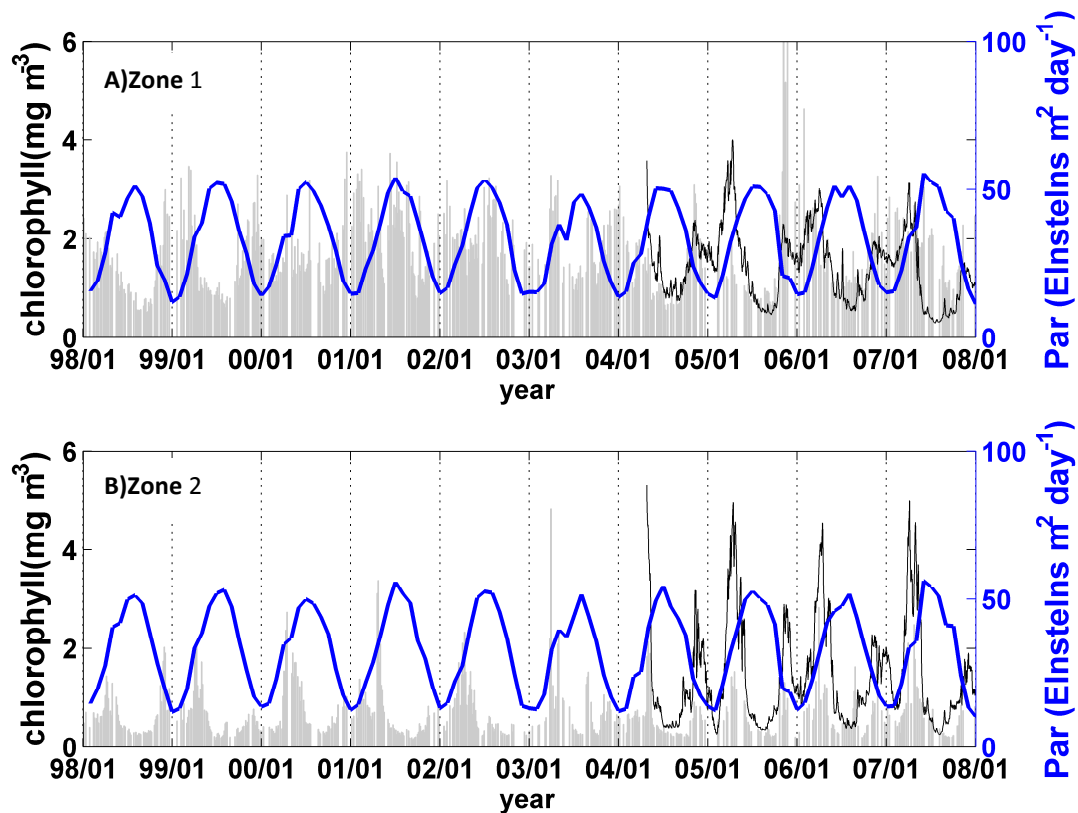


Figure 3. 2. The nine-year record of SeaWiFS chlorophyll (bar) compared to photosynthetically active radiation (PAR, blue line) from the spatial mean in (A) Zone1 and (B) Zone2. The black line overlapped is the model simulated spatial mean chlorophyll in Zone 1 and Zone 2.

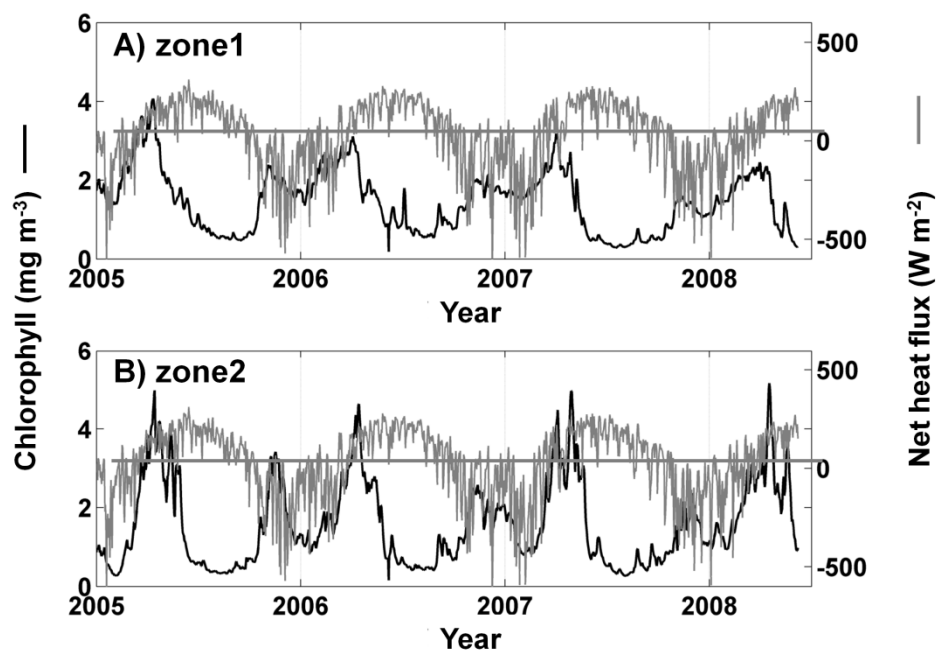


Figure 3. 3. Time series of surface chlorophyll concentration (black line) and net heat flux (grey line) of spatial mean in Zone 1 and Zone 2 calculated from model output.

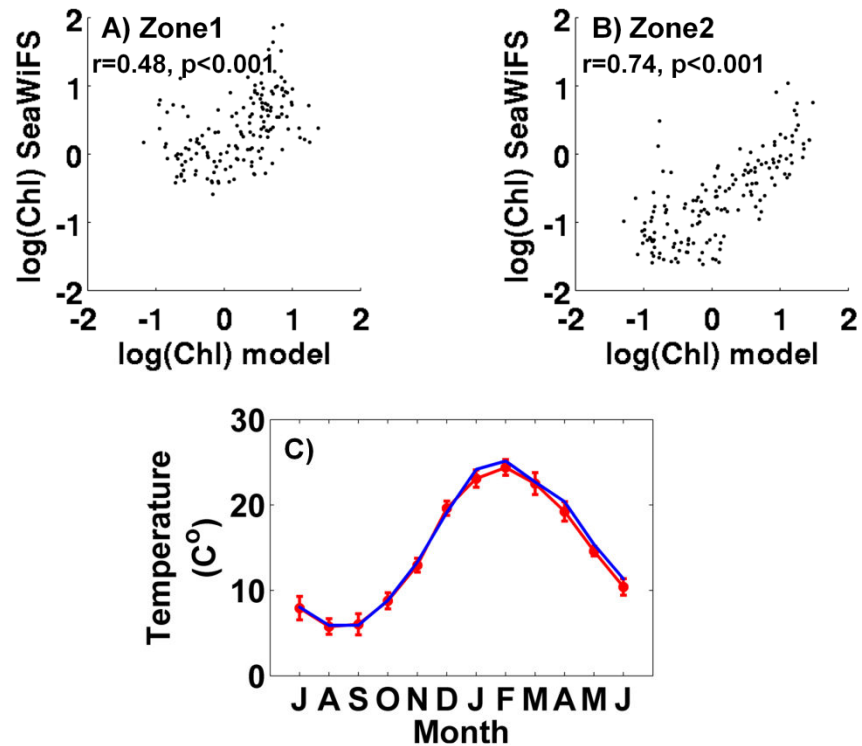


Figure 3. 4. Comparison between the log-transformed surface chlorophyll concentrations provide by SeaWiFS and mode output from spatial mean of Zone 1 and Zone 2. The linear correlation of the chlorophyll before log-transformed is 0.42 and 0.75 (P value <0.001) for Zone 1 and Zone 2 respectively. The climatology of surface water temperature from the NDBC buoy 44009 (the red line with error bar) was used to compare with the simulated SST at the same location (blue line) in Figure 4C.

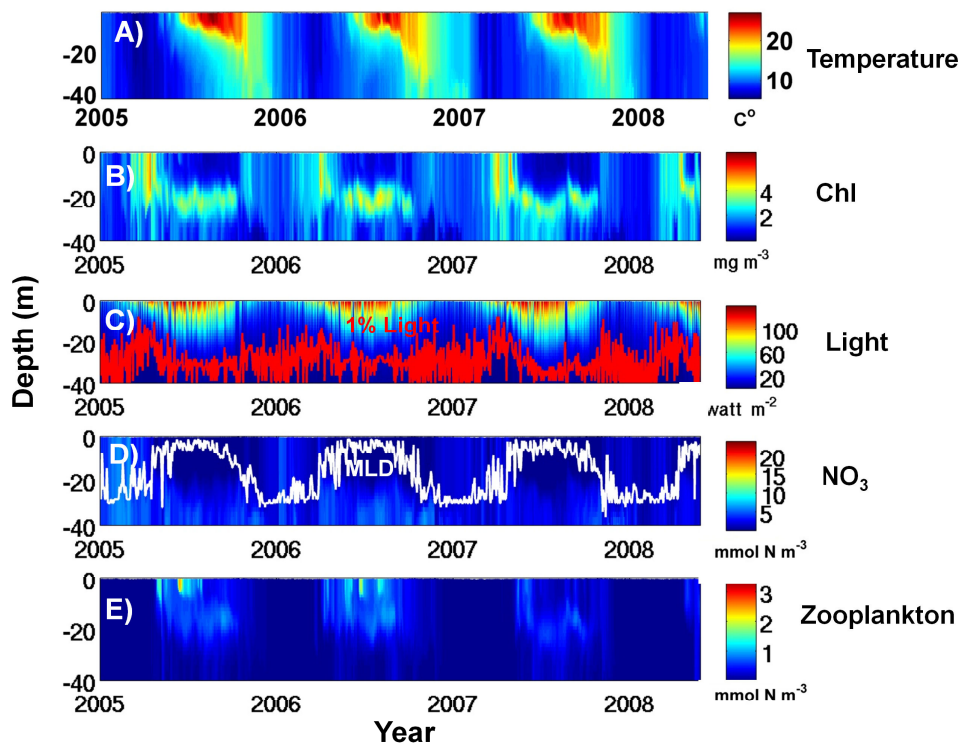


Figure 3. 5. Model simulated vertical distribution of temperature (A) chlorophyll concentration (B), light (C), NO₃ (D) and zooplankton (E) at a point located in Zone 1 (dot shown in Figure 1). The 1% light level depth is plotted with light (in C, red line) and the MLD is plotted with NO₃ (in (D), white line).

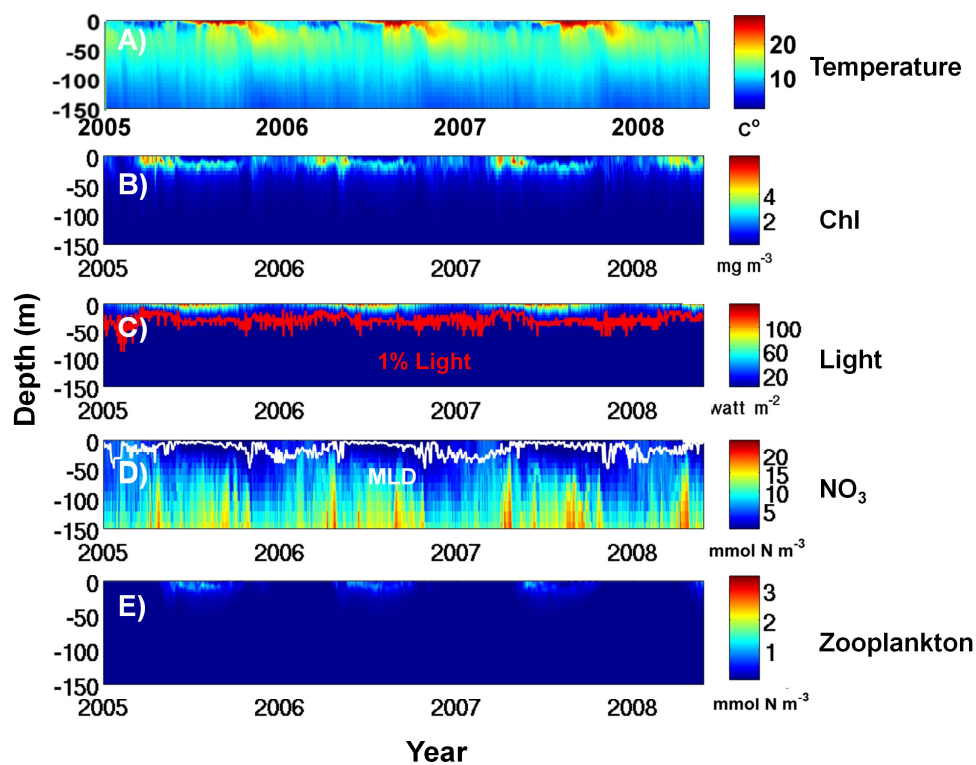


Figure 3.6. Model simulated vertical distribution of temperature (A) chlorophyll concentration (B), light (C), NO_3 (D) and zooplankton (E) at a point located in Zone 2 (square shown in Figure 1). The 1% light level depth is plotted with light (in C red line) and the MLD is plotted with NO_3 (in D, white line). (Here, we only show the upper 150 m of the water column).

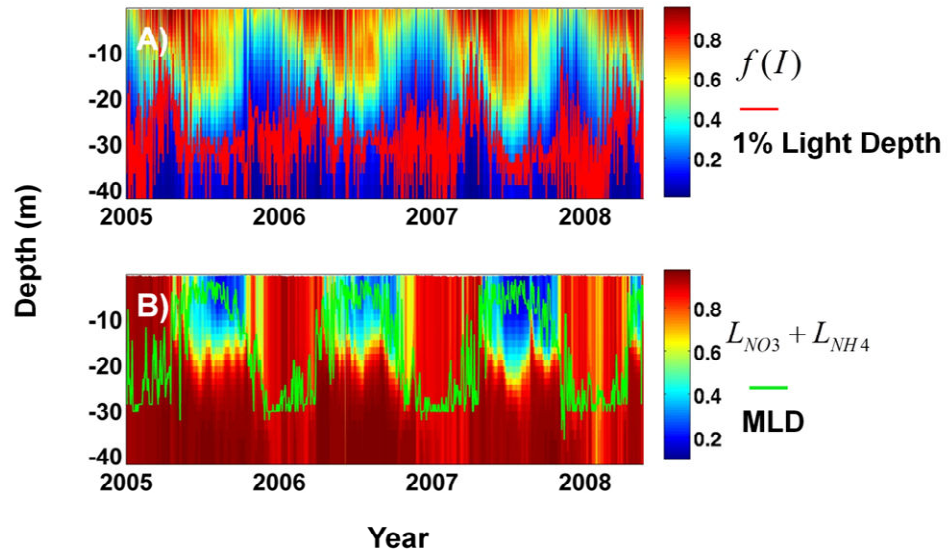


Figure 3. 7. Vertical distribution of limitation function of light (A) and nutrient (B) at a point located in Zone 1 (dot shown in Figure 1). The 1% light level depth is plotted with function of light (in A, red line) and the MLD is plotted with nutrient limitation function (in (B), green line).

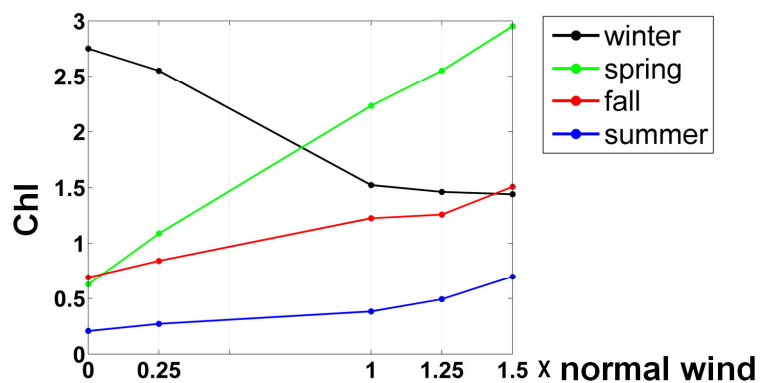


Figure 3. 8. Spatial mean chlorophyll in Zone 1 under different scale of wind

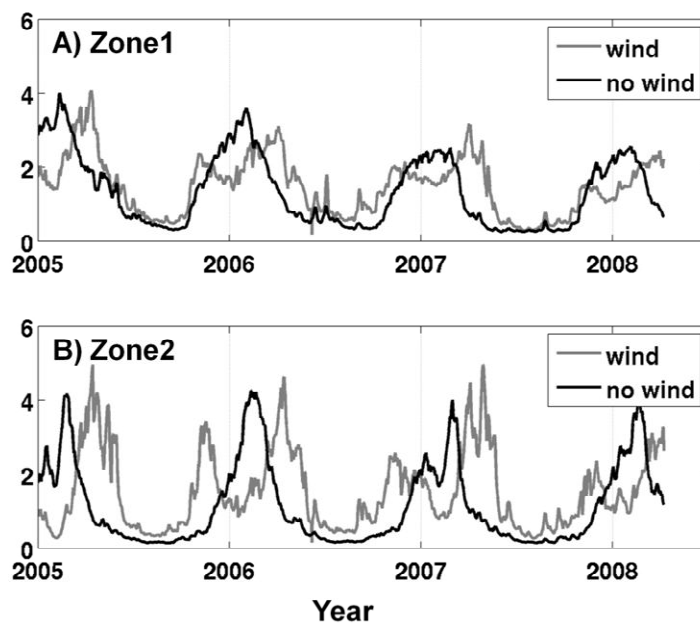


Figure 3. 9. Simulated time series of spatial mean surface chlorophyll concentration in Zone 1(A) and Zone 2(B). Black line represents the result under normal wind conditions; grey line represents the “no wind” forcing result.

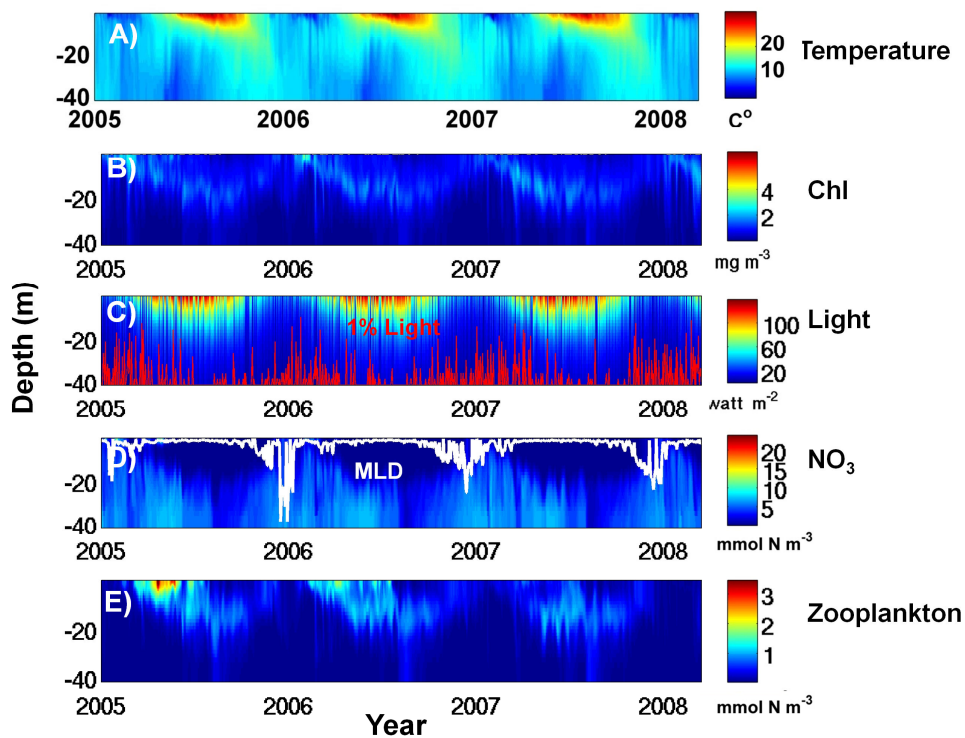


Figure 3. 10. Without wind forcing, the simulated vertical distribution of temperature (A) chlorophyll concentration (B), light (C), NO_3 (D) and zooplankton (E) in a dot located in Zone 1(dot shown in Figure 1). The 1% light level depth is plotted with light (in C, red line) and the MLD is plotted with NO_3 (in (D), white line)

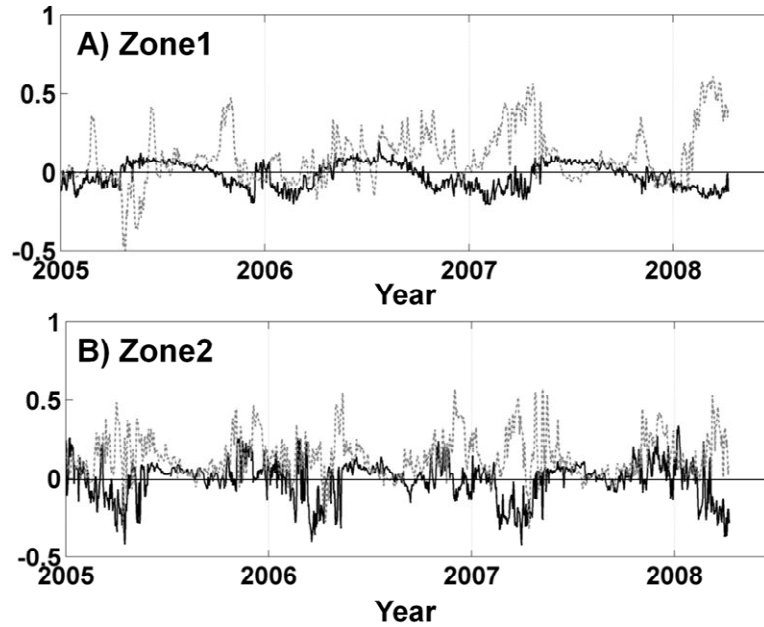


Figure 3. 11. Difference (normal wind – no wind) of mixed layer mean light (black line) and nutrient (gray dashed line) limitation function between normal wind and no wind forcing condition in (A) Zone 1 and (B) Zone 2. For Zone 1, negative light function difference value in winter represents the decrease of light limitation under no wind condition.

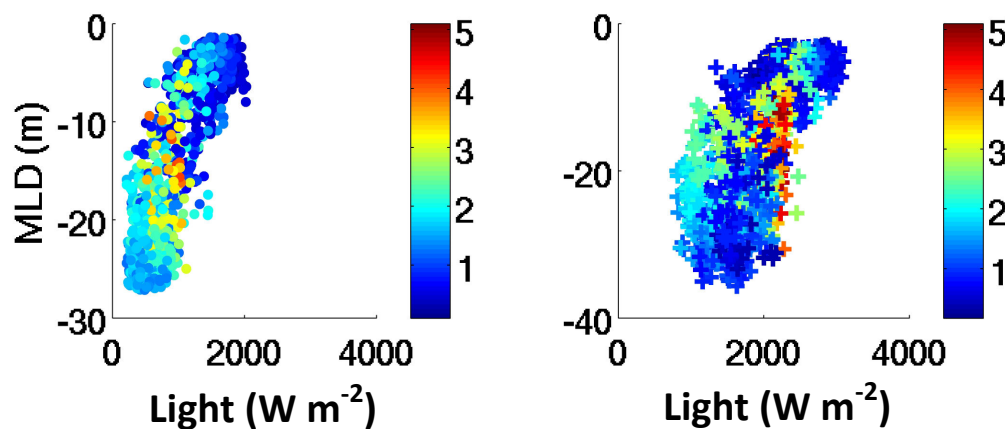


Figure 3. 12. Scatter plot of modeled mean light value in the mixed layer with MLD in Zone 1 (a) and Zone 2 (b). The color represents the chlorophyll concentration (mg m^{-3}).

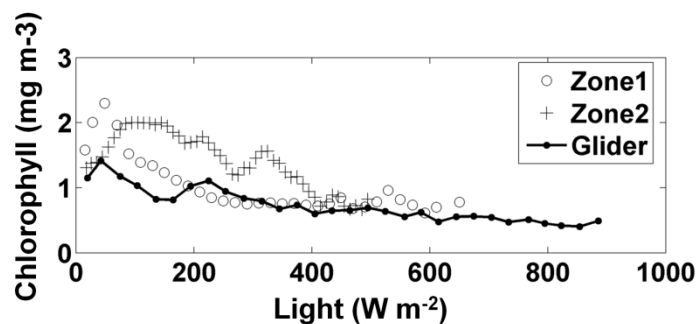


Figure 3. 13. Simulated mixed depth mean chlorophyll concentration and I' in every 20 W m^{-2} . I' value bins in Zone 1 (grey circle line) and Zone 2 (grey plus line), chlorophyll and I' based on glider observation are shown in black line with dots.

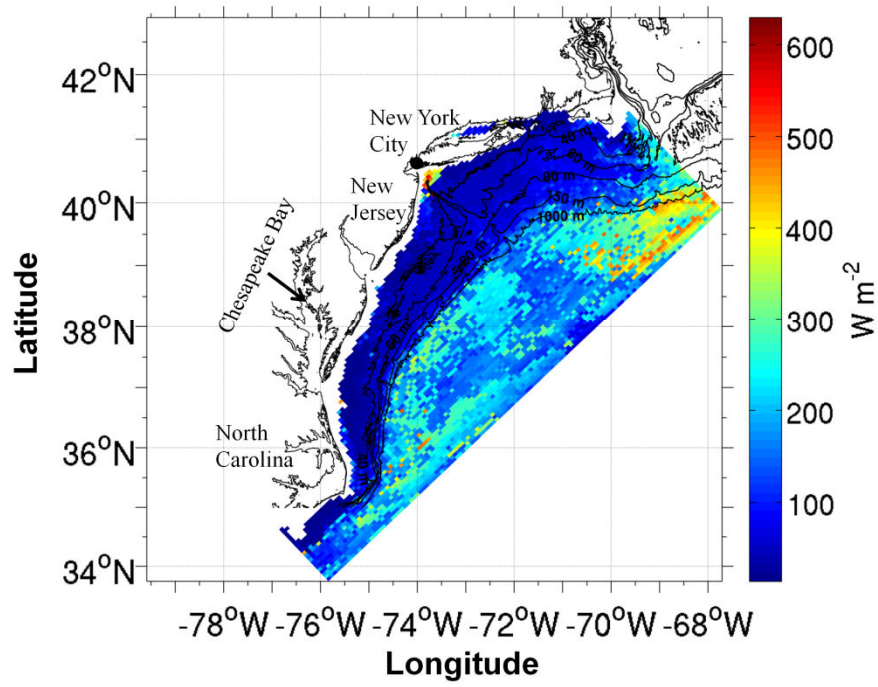


Figure 3. 14. The critical light value ($I'_{chl \max}$) in each grid of model domain.

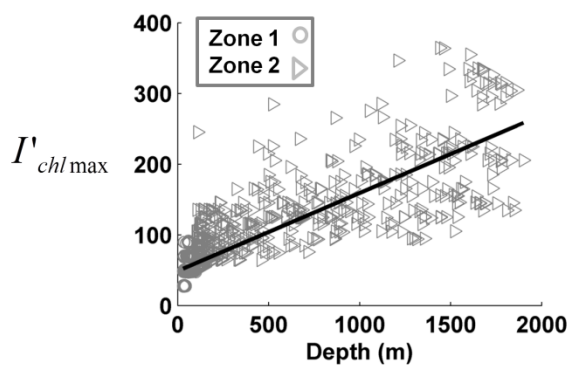


Figure 3. 15. The relationship between the critical light value and water depth of all grids in the MAB. We separate grids in Zone 1 and Zone 2 with circle and triangle individually. Black line represents the linear regression of water depth and critical light value.

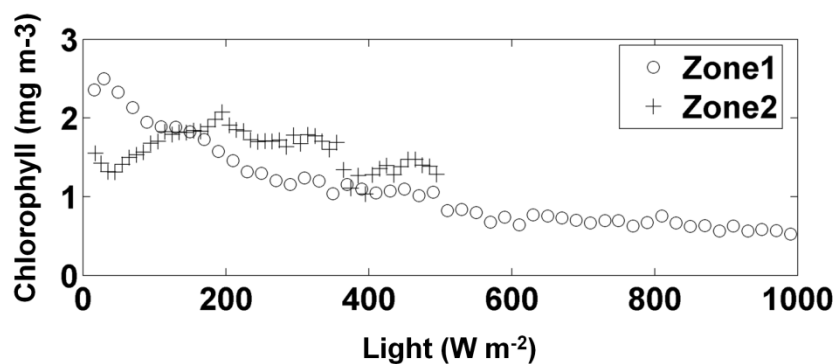


Figure 3. 16. Under no wind forcing, simulated mixed depth mean chlorophyll concentration and I' in every 20 W m⁻² I' value bins in Zone 1 (red circle line) and Zone 2 (blue circle line), chlorophyll and I' based on glider observations are shown in black line with dots.

CHAPTER 4. DECADAL VARIABILITY OF CLIMATE AND WINTER

PHYTOPLANKTON BLOOM IN THE MID-ATLANTIC BIGHT

4. 1. Introduction

The water in the Middle Atlantic Bight (MAB) undergoes significant decadal variability in the temperature and salinity. Based on the hydrographic data during the period 1997-1999 from the Northeast Fisheries Science Center (NEFSC) MARMAP program, Mountain (2003) have shown that the MAB shelf has been 1°C warmer and 0.25 PSU fresher in the 1990s than during the 1977-1987 period. Long records (1875–2007) of temperature data over the US continental shelf along the east coast indicate that substantial interannual variability of temperatures arises due to advection from the north (Shearman and Lentz, 2010). Some of those variabilities are associated with the Atlantic Multidecadal Oscillation (AMO) which is an index based on the anomaly of the sea-surface temperature in the North Atlantic with characteristic time scales of 50–100 yr. The AMO index correlates with various climatic characteristics: air temperature, river discharge in the European and North-American regions, the number and intensity of tropical cyclones in the Atlantic Ocean, and the parameters of mid-latitude cyclones and anticyclones in the Atlantic–European region (Enfield and Mestas-Nunez, 1999; Kerr, 2000; Enfield and Cid-Serrano, 2010). Other indexes such as the North Atlantic Oscillation (NAO) or the Multivariate ENSO Index do not exhibit such local spatial patterns, and their typical scales of variations are much shorter, which makes them inappropriate for the present multidecadal analysis (Martinez et al., 2009). In this study we examine the multidecadal behaviors of weather forcing over the MAB as they relate to the alternating phases of the oceanic AMO.

Chlorophyll a (chl a) concentrations in the MAB appears to have declined over the last three decades based on ocean color satellite data (Schofield et al., 2008). The changes vary with the season in the MAB. The fall and winter seasons show declines in chl a (43 and 29%, respectively), while the spring and summer months show small increases (8 and 14%, respectively). The annual change in the MAB chlorophyll is around -14% driven by the decline in the fall/winter blooms which account for 63% of the annual chl a on the MAB (Yoder et al., 2002; Xu et al., 2011). Declines in chl a appear to be distributed over the entire shelf, which implies that the underlying processes must operate over the entire MAB.

The major physical feature regulating overall annual primary productivity of the MAB is the seasonal stratification of the shelf. Phytoplankton biomass on the MAB is low after the shelf has stratified in spring as nutrients are rapidly depleted in the euphotic zone (Xu et al., 2011); therefore, it is not surprising that the largest phytoplankton blooms on the MAB occur during the late fall and winter seasons (Ryan et al., 1999; Yoder et al., 2002) when frequent storms and the seasonal cooling erodes the shelf stratification and nutrients in the euphotic zone are regularly replenished. Spatially, winter blooms are confined on the inner half of the MAB shelf, and the magnitude of the winter bloom appears to be inversely correlated with the number of stormy days on the MAB (Xu et al., 2011), consistent with light limitation being the critical variable driving phytoplankton growth (Xu et al., 2011; 2012). Therefore factors predicted to alter water stability are expected to significantly impact the primary productivity.

For the continental shelf of the MAB, very few sufficiently long biological time series exist to assess interannual to decadal variability of phytoplankton blooms.

Although it is not possible to detect decade-scale variability by using the longest currently-operating SeaWiFS data alone, by comparing climatological SeaWiFS data against data from the CZCS, which operated between 1979 and 1985 one can detect long-term trends in marine biology due to climate change. Understanding past variability in bloom dynamics and the associated physical mechanisms is a key to predict how ocean biology will respond to climate change. As we know, phytoplankton blooms in the coastal ocean of MAB are mainly regulated by stratification which is the dominant feature resulting the balance between light and nutrient limitation for phytoplankton growth (Xu, et al., 2011). Here, we seek to understand the mechanisms by which process dominant water column stability in the MAB and the mechanistic connections between regional and interannual/decadal meteorological change which may be associated with broader scale patterns of shifting climates regimes and their influence on biological productivity. To understand how these processes may underlie the decadal declines in chl a during the shift to a AMO+, we will focus on quantifying the relative importance of these multiple mechanisms in regulating water column stability using a biogeochemical model and coupling those results to ocean and meteorological time series data.

4. 2. Data, Model, and Methods

4. 3. 1. Ocean color remote sensing data

Time series of surface chl a in the MAB was studied using monthly-averaged composites of 5.5-km resolution CZCS and SeaWiFS data collected from January 1979 to December 1985 and January 1998 to December 2006 respectively. Given the spatial heterogeneity in the nearshore waters and increasing error in satellite estimates of chlorophyll in shallow waters, we excluded regions with water depths shallower than 20

m for this analysis. We also excluded data for water depths deeper than 2000 m, as our focus was on the shelf and shelf-break region. Images with more than 20% of cloud pixels were removed. For the valid images, pixels covered by clouds were replaced by the average of the surrounding 8 non-cloud pixels. From the monthly averages, we compute monthly special mean anomalies.

4. 3. 2. Meteorology data

Wind and water properties data were obtained from moored buoys deployed by the National Data Buoy Center (NDBC). The moorings 44025, 44008, 44011 and 44009 were used. We calculated the net heat flux using the NDBC buoy data to make bulk heat flux estimates (Fairall et al., 1996). The shortwave and longwave radiation data used in this calculation were obtained from National Solar Radiation Data Base (http://rredc.nrel.gov/solar/old_data/nsrdb/). The Atlantic City site was chosen since it is the closest station near NDBC buoy 44009. The daily river discharge data from 1975 to 2007 was downloaded from <http://nwis.waterdata.usgs.gov/nwis>. The total river discharge into to the MAB was represented by the sum of the discharges from Mohawk River at Cohoes, NY; Passaic River at Little Falls, NJ; Raritan River below Calco Dam at Bound Brook, NJ; Hudson River at Fort Edward, NY and Delaware River at Trenton, NJ.

4. 3. 3. Biogeochemical Model

We used a biogeochemical model developed by Fennel et al. (2006), which is integrated with the ROMS (Haidvogel and Beckmann, 1999; Wilkin et al., 2005; Xu et al., 2012). We conducted 4-yr simulations (2004-2008), but use the results from the years 2005-2006 here. To test the sensitivity of forcing on water column stability and the

corresponding influence on phytoplankton activity, we conducted five different simulations. The first simulation is with all the normal forces (measured rivers, wind stress, and net heat flux). Four additional simulations were carried out to investigate the individual effects of net heat flux, wind, and river discharge on the timing and magnitude of phytoplankton blooms.

4. 3. Results

4. 3. 1. Terms influencing water column stability

Phytoplankton dynamics on the MAB is driven by the overall stratification of the water column. The three most important factors in determining the overall water column stability in the MAB is the interannual variability in the freshwater input, winds and solar heating. Assuming that the stratifying effect of buoyancy inputs and the mixing produced through winds and tides act independently, the competition between these influences determine overall water column stratification. In order to assess the balance between the processes that mix the water column to those that stabilize it, we calculate the potential energy anomaly (PEA) of the water column and use its diagnostic terms to investigate the water column stability. Simpson et al. (1977) (see also Simpson and Bowers, 1981) define the anomaly of potential energy as

$$\phi = \frac{1}{D} \int_{-H}^{\eta} gz(\bar{\rho} - \rho)dz, \quad (7)$$

where $\bar{\rho}$ is the depth-mean density,

$$\bar{\rho} = \frac{1}{D} \int_{-H}^{\eta} \rho dz, \quad (8)$$

The PEA is zero for a fully mixed water column, positive for stable stratification and negative for unstable stratification. Physically, PEA gives the amount of energy per volume that is necessary to vertically homogenize the entire water column. To determine whether the water column remains stratified or mixes as a result of the forcing acting on the water column, we calculated the change of PEA with time:

$$\frac{d\phi}{dt} = \frac{\alpha g Q}{2c} + \frac{g(E - P)\Delta\rho}{2} - \varepsilon k_b \rho \overline{|u_b|^3} - \delta k_s \rho_s \frac{\overline{W^3}}{h} + \frac{g}{h} \frac{\partial \rho}{\partial y} \int_{-h}^0 (v - \hat{v}) z dz, \quad (9)$$

The first two terms on the right represent the change of water column stability due to surface heat at a rate Q and salt flux due to evaporation (E) and precipitation (P), while the third and fourth terms are due to stirring by tide current (u_b) and wind of speed (W). Here, ε and δ are the corresponding mixing efficiencies and k_s and k_b are the effective drag coefficients for surface and bottom stresses. α and c are the thermal expansion coefficient and specific heat of seawater and ρ_s is the density of air. The last term represents the influence of freshwater input from rivers on the water column stability. For horizontal flows across the shelf (in the y direction), the density gradients across the shelf drive a shear flow circulation with low-density water flowing offshore at the surface. The contribution of such shear on PEA can be represented as the last term, which allows us to calculate the input of ϕ for any known velocity field u . The order of magnitudes of each term represents the importance for the input to ϕ (Figure 4.1). The heat flux, wind mixing and river runoff term have the same order of magnitudes, while the tidal mixing and salt flux term is much less. So, the heat flux, wind mixing and river

runoff term can be considered as the major sources for stratification and destratification in MAB.

4. 3. 2. Model sensitivity study

We conducted a serial of model sensitivity studies to assess the importance of the timing and magnitude of phytoplankton blooms based on changes in the processes influencing the relative balance between nutrients and light limitation in phytoplankton bloom. The river runoff not only inputs buoyancy by providing low salinity water but also provides high concentrations of nutrients to the continental shelf (Moline et al., 2008). Therefore we conducted two sensitivity experiments to study the respective roles of the river on phytoplankton growth. In Experiment 1, no river input was included in the model simulation. In Experiment 2, we kept the river input as temperature and salinity sources/sinks and mass sources/sinks terms, but turn off the input of nutrients from river. Experiments 3 and 4 were used to assess the importance of the net heat flux and wind mixing on phytoplankton blooms by omitting these processes in the simulations. The four experiments results are compared with the “normal” model conditions which included all the forcing factors.

The model simulations showed that the timing of the destratification and initiation of fall bloom was closely related to the wind forcing. When the wind forcing was turned off in the model, the timing of the breakdown of shelf stratification and initiation of fall bloom was delayed (Figure 4.2 red line). Additionally, there was significant decrease of chlorophyll. In contrast, when the net heat flux was turned off there was no decline in the chlorophyll. This suggests the breakdown of the seasonal thermocline, and subsequent

replenishment of the nutrients in the euphotic zone, and the resulting bloom was primarily due to wind forcing.

In the winter months, there was a significant increase in the magnitude of the bloom when the no wind condition and no net heat flux scenarios were applied. The ‘no wind’ and ‘no cooling’ conditions decreased mixing and allowed for larger winter blooms as a result of lower mixing and the corresponding increase in light availability (Xu et al., 2012). The concentration of chlorophyll did not change when the nutrient inputs from rivers were turned off. While the river nutrients did not appear to play a major role in increasing the phytoplankton productivity, the river’s role increasing water stability was significant. This was evidenced by the decrease of chl a for all seasons when the input of low salinity water was turned off. The river inputs did significantly impact the timing and magnitude of the fall bloom.

4. 3. 3. Decadal variability of Chlorophyll

The CZCS and SeaWiFS missions spanned negative and positive AMO cycles (AMO-, AMO+) respectively. The average chlorophyll concentration for the whole MAB decreased in the fall to winter months during the AMO+ period by 2-3 mg m⁻³ (Figure 4.3a). There was an increase in summer during the years 2000 to 2003 by 1 mg m⁻³ (Figure 4.3a). The average, and standard deviations, of chlorophyll during the AMO- (CZCS) and AMO+ (SeaWiFS) was calculated (Figure 4.3b). Chlorophyll exhibited a climatological maximum value of 3 mg m⁻³ in winter. AMO- winters have chlorophyll concentrations of ~5 mg m⁻³, whereas AMO+ winters exhibited concentration ~2 mg m⁻³. The variability in the winter blooms accounted for most of the standard deviation in the annual chlorophyll concentration (Figure 4.3b).

Empirical orthogonal function (EOF) was calculated over the combined CZCS-SeaWiFS data sets in order to determine the dominant modes of variability for the MAB. The seasonal signal in the monthly chlorophyll monthly was removed prior to the EOF analyses. Each anomaly data set is divided by its standard deviation. The first dominant EOF explained 31% of the total variance. All the spatial coefficients were negative (Figure 4.3c). The temporal signal reverses from negative to positive from 1979–1986 to 1998–2006 (Figure 4.3d). Consequently, when they were multiplied by temporal amplitudes the whole chlorophyll field decreased. This corresponds to a shift of the AMO index from a cool to a warm phase in the late 1990s. Consequently, when temporal amplitudes were multiplied by negative spatial coefficients the whole field decreased during the AMO+ period with respect to the chlorophyll climatology. For the fall-winter bloom, the declines in chlorophyll reflected changes in the overall water column stability due to altered wind, river discharge that are affected by the AMO index (Xu et al., 2011).

4. 3. 4. Decadal variability of Meteorological Forcing.

The model simulations clearly demonstrate that in the MAB, phytoplankton growth is the balance between light and nutrient limitation and the corresponding changes in water column stratification. Any change of stratification may potentially affect phytoplankton growth, which may happen at different spatial and temporal scales. On seasonal to interannual time scales, there are changes of the wind stress, SST, river discharge and any other factors related with stratification.

a. Wind

Here we examined in situ and model re-analysis time-series wind data in the MAB. The frequency of storms during winter (December to February) was determined

from four NDBC Moored Buoys for the period 1983 to 2010 with the time periods cover the CZCS and SeaWiFS time (Figure 4.4). A stormy day was defined as one on which the wind speed was greater than 10 m s^{-1} . The time-series of stormy frequency shows there is an increase trend of stormy time during winter. The 2004-2008 period experienced more winter storms than the 1983-1986 period showing from the station of 44008 and 44009 where they are not closed in location (44008 located near Southeast of Nantucket and 44009 located in the Southeast of Cape May, NJ). The climatology of storm frequency of 44008 and 44009 for those two time periods show there are more storms during December to February especially in January in the period of 2004-2008 (Figure 4.5 a,b). The North American Mesoscale (NAM) forecast system from the National Centers for Environmental Prediction (NCEP) re-analysis data (Mesinger et al. 2006) which we used to force the model are used to compare with the NDBC buoys. We pick out two grid points with close longitude and latitude with the two NDBC buoys from the NCEP data sets for the same time periods. The climatology results also show the same trend (figure 4.5 c,d) with higher storm frequency during the 2004-2008 period in winter.

b. Temperature, salinity and net heat flux

Another important factor influencing water column stability is water temperature and salinity. The change of water temperature can influence the surface atmospheric heat flux so as to affect the vertical exchange of heat and water column stability. For the winter time, the NCEP sea surface temperature and salinity data in January shows there are increase of sea surface temperature over the whole MAB but decrease of salinity in the estuary (Figure 4.6). The climatology of water and air temperature for the station 44009 confirms the increase of water temperature during winter for the time period of

2004-2008 (Figure 4.7a, b). The standardized net heat flux anomaly shows more heat loss in the 1995-2005 years especially in winter time (Figure 4.8). This increase in heat loss could either be because of the increasing wind stress or the higher air-sea surface temperature difference, however, the result is more mixing caused by heat loss in the water column.

c. River discharge

The analyses of climatology USGS river discharge presents that there are higher river discharges in the 2004-2008 year especially in January (figure 4.8), which confirm with the NCEP data (Figure 4.6 b) that there is significant changes of salinity mostly near the estuary in winter implying more fresh water input from river.

On seasonal to interannual time scales, there are changes of the wind stress, SST, river discharge and any other factors related with stratification. Here we examined the observed wind, net heat flux, and river discharge data and compared their normalized distribution with AMO index for 1985-2010 by seasons. The AMO- to AMO+ transition has altered the wind forcing, net heat flux, and river discharge rates in the MAB (Figure 4.9, Table 4.1).

There have been shifts that will impact the timing of the fall bloom. The wind stress in the fall and winter season have increased by 4% and wind speeds are significantly correlated with the AMO- to AMO+ transition ($r = 0.55$, $P < 0.005$). While there was no significant correlation between AMO to river discharge or net heat flux during the fall season, there was an increase in the river discharge (34%) and heat flux (42%). The model sensitivity studies demonstrated that the wind and river discharge had

larger affects on phytoplankton growth, more than changes in the net heat flux. The increase of wind stress would enhance destratification, which would increase chlorophyll concentration in fall; however in contrast the increase in river discharge would stabilize the water column and inhibit the water column mixing. The increase in river discharge would thus delay and decrease the magnitude of the fall bloom. Ocean color observations suggest that the fall chlorophyll concentrations have declined by 53%. This would suggest that an increase in river discharge is the primary driver influencing changes in the fall phytoplankton bloom.

In contrast to the fall, in the winter season the wind, net heat flux, and river discharge all significantly affect chlorophyll concentration. The wind stress increase (3%) was significantly correlated with the AMO index with a correlation coefficient of $r = 0.59$ ($P < 0.001$). This increase in wind would lead to a decrease of the phytoplankton concentrations by increasing mixing and light-limitation during the winter months (Xu et al., 2012). This effect would be magnified by the observed declines of the ocean heat flux (5%). The associated increase in winter river discharge (12%) would contribute to the water column stability and would lead to an increase in phytoplankton growth in the winter months. The ocean color data shows the winter chlorophyll has decreased by 41%, which would suggest that increase of wind and increased heat loss to the atmosphere were larger effects than the winter time river discharge in influencing the overall water column stability on the inner shelf of the MAB (Xu et al., 2011).

In spring, there were no significant correlations between the AMO index and the three terms influencing PEA. There was no significant change in wind stress and a small 7% decrease in the river discharge (Figure 4.4c). There is a larger decrease of heat flux

into the ocean during a positive AMO period (93.9%) and the decrease of chlorophyll (7.5%) could reflect delayed of stratification due to slower rates of water column stabilization and decreased river discharge.

The only significant increase in chlorophyll concentration during the positive AMO was in the summer season (12%). Observations in the summer, suggest that wind stress decreased by 3.2%, which combined with the increase of river discharge (13.7%) would suggest increased stratification during the summer in the MAB. Therefore another factor must drive the increase in chl *a*. During the summer, southwest winds associated with the Bermuda High are associated with coastal upwelling, which results in significant phytoplankton blooms (Glenn et al., 2004) that can cover a significant fraction of the MAB (Moline et al., 2004). During the transition to AMO+ there has been an increase in the number of summer months that have winds that are upwelling favorable. During the AMO- there was an 85% probability that summer months were dominated by upwelling favorable wind, however since transition to the AMO+ mode the probability of summer upwelling favorable has increased to 97%. Thus while overall wind stress has decreased, the increased upwelling might account for the increased summer phytoplankton concentrations.

4. 4. Conclusion

We investigated the decadal variability of chlorophyll concentration in MAB by comparing the monthly averaged chlorophyll during CZCS and SeaWiFS periods which experience the negative and positive AMO respectively. Our results demonstrate that substantial decadal variability of chlorophyll concentration occurs in response to variability of forcing. The bio-physical model is able to reproduce the seasonal fall-

winter bloom and the timing and magnitude of the bloom is influenced by different forcing in various certain extents. Although the well-known correlation between the phase of the AMO and atmospheric condition has long been hypothesized to affect phytoplankton blooms in global and basin-scale, the lack of high-resolution, long-term biological records has presented difficulties in investigating the relationships in local coastal area like MAB. This study, by combination of satellite data, observations and model output, quantifies the relationship between forcing and decadal variability in timing and magnitude of phytoplankton bloom and the impact of the AMO on the change of forcing in the MAB.

In conclusion, the transition to an AMO+ has resulted in an overall decline in MAB chl a. The changes in chl a varied with season. The largest declines are observed in the fall and winter seasons. The declines in fall are driven by an increase in river discharge which delays the onset of the winter bloom. The decline in the winter bloom is driven by increased wind stress and decreased heat fluxes, which also delays the start of the spring bloom that requires stratification for initiation. Finally the increase in upwelling favorable winds drives the increased chl a in the summer months.

Table 4. 1. Percentage change of wind, river, net heat flux and chlorophyll from AMO- period to AMO+ period. Positive means increase, negative means decrease.

	Fall	Winter	Spring	Summer
Wind (%)	3.6	3.1	0.7	-3.2
River (%)	33.7	12.3	-6.9	13.7
Net heat flux (%)	41.8	4.6	-93.9	-23.7
Chl α(%)	-53.4	-40.8	-7.5	11.7

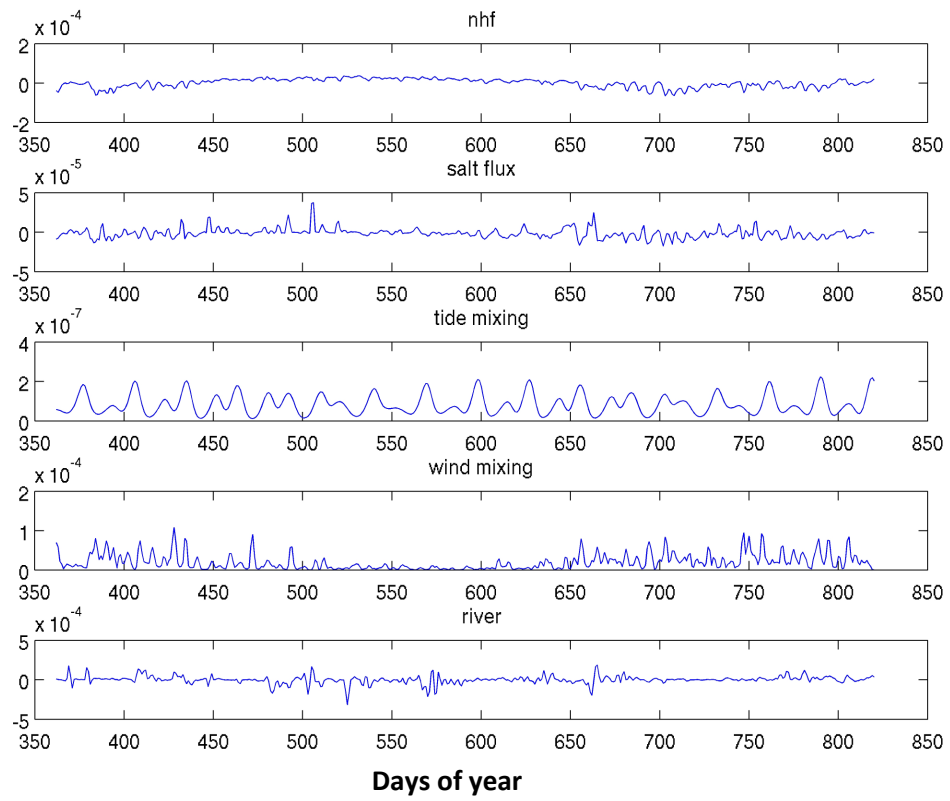


Figure 4. 1. Time serials of change of PEA with time in equation (9).

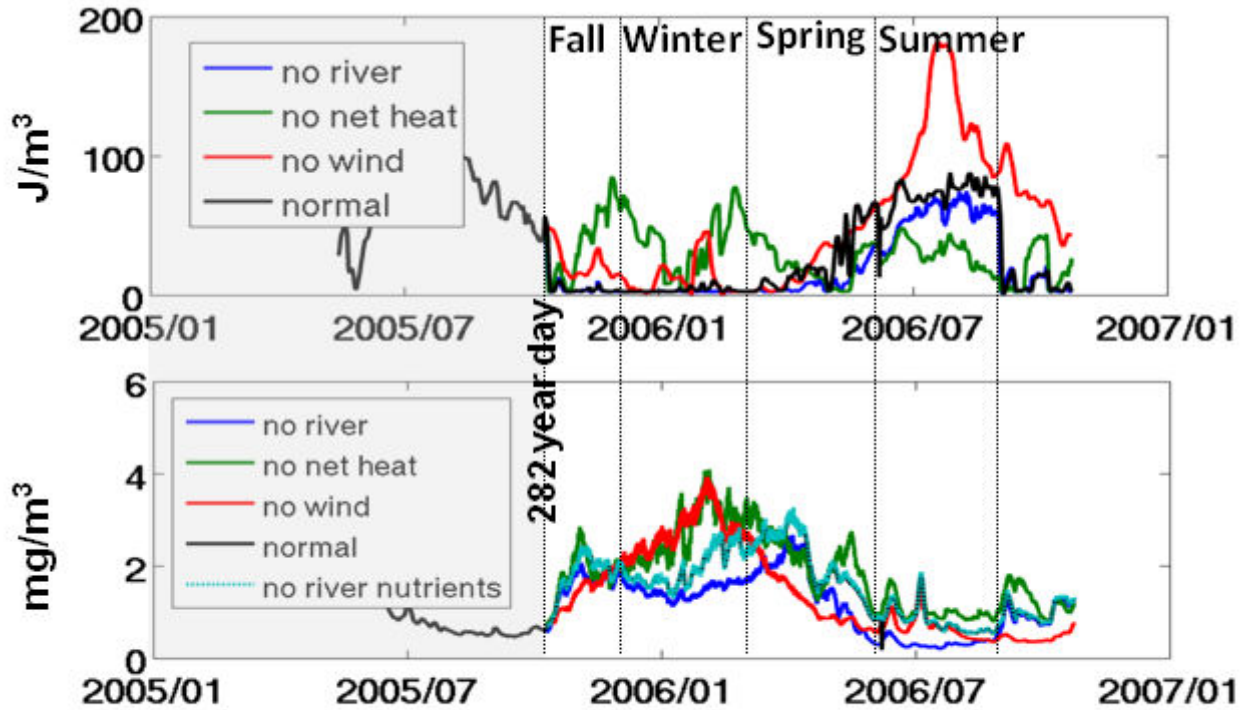


Figure 4. 2. Model sensitivity study results of the time serials of Zone 1 spatial mean PEA (a) and chl a (b) under different forcing. In the Experiment of ‘no wind’ and ‘no net heat flux’, the wind and net heat flux are turned off at the day (around the 282 day of year 2005) when the neat heat flux changes from positive to negative (Here we only compare the results after that day). The normal condition results are shown in black line. In the PEA lot, the black line is overlapped partially with the no river condition in winter; in the chl a plot, the black line is overlapped with no river nutrients input condition (light blue line).

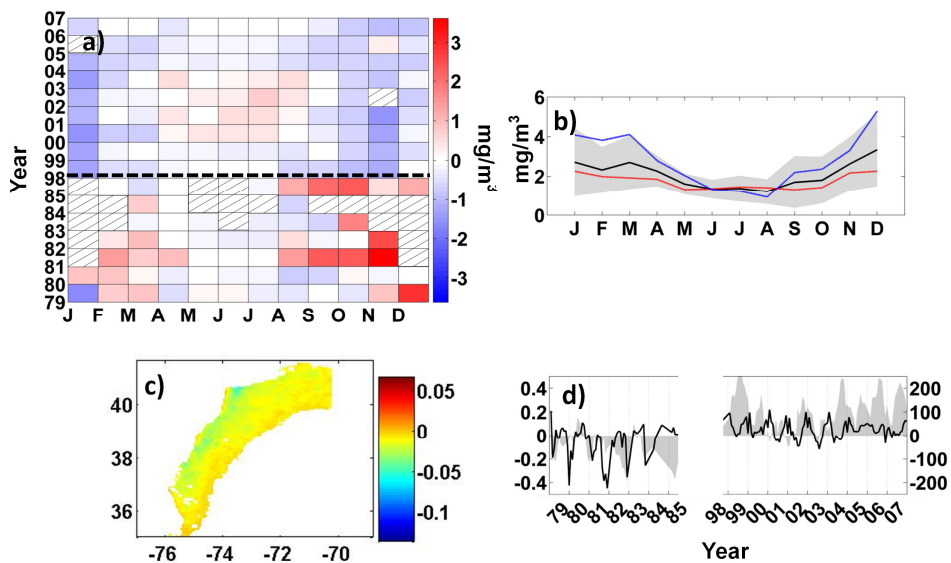


Figure 4. 3. Decadal variability of chl a. (a) Monthly average chl a anomalies, blank window means there is no available data at this month. (b) Climatological seasonal cycles in chl a (black), their standard deviation (gray shading), AMO+ composites (red dashed line), and AMO- composites (blue dashed line). (c) Spatial coefficients of EOF mode 1. (d) CZCS-SeaWiFS chl a time variability of EOF mode 1 (black). AMO index is superimposed as gray shading.

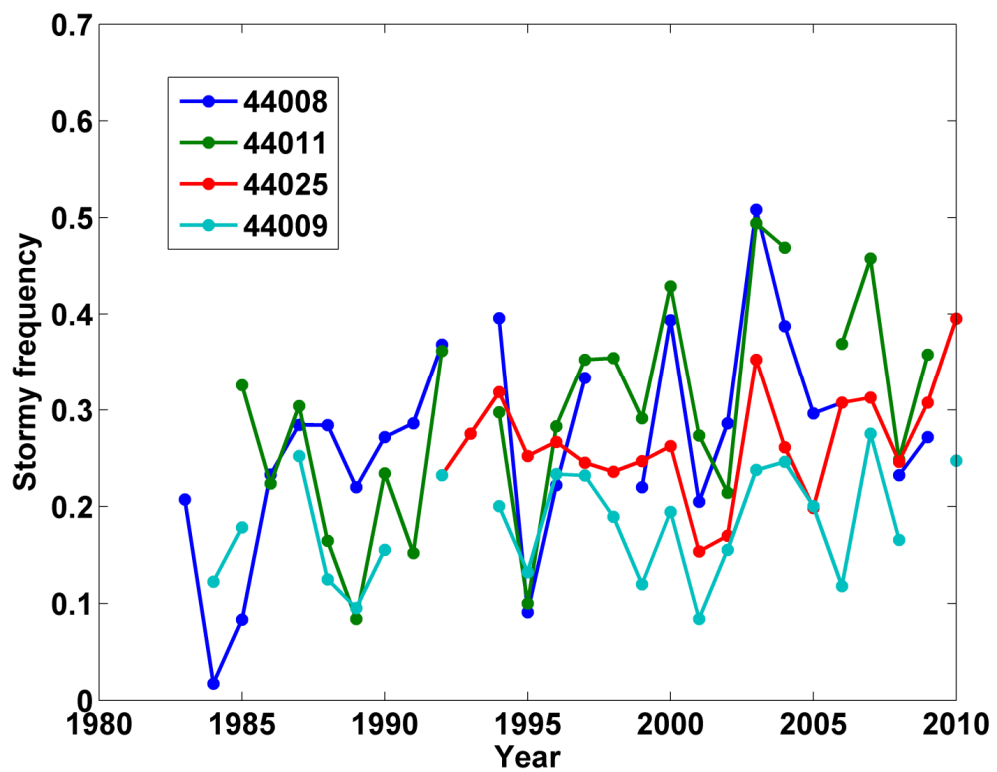


Figure 4. 4. Winter time storm frequency for the NDBC buoys 44008, 44011, 44025, and 44009.

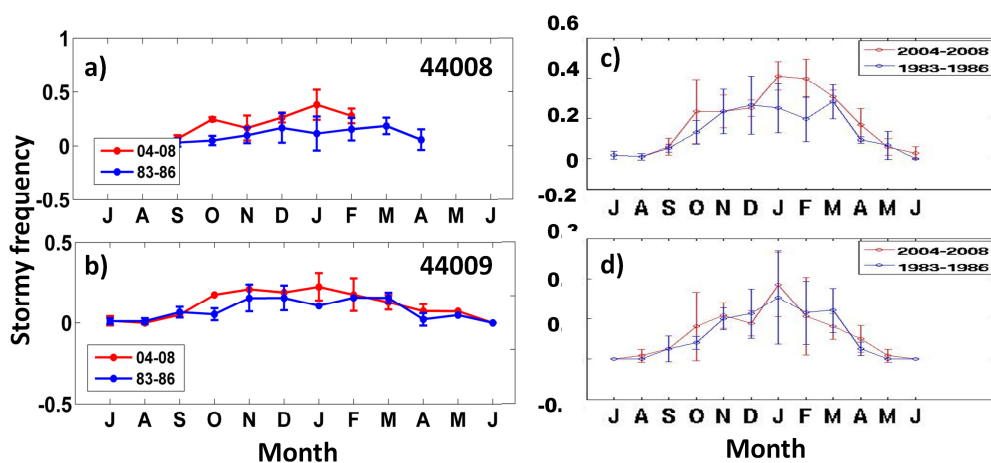


Figure 4. 5. The climatology of storm frequency of 44008 and 44009 NDBC moored buoys(a,b) and NCEP data at the same location (c,d)for those two time periods.

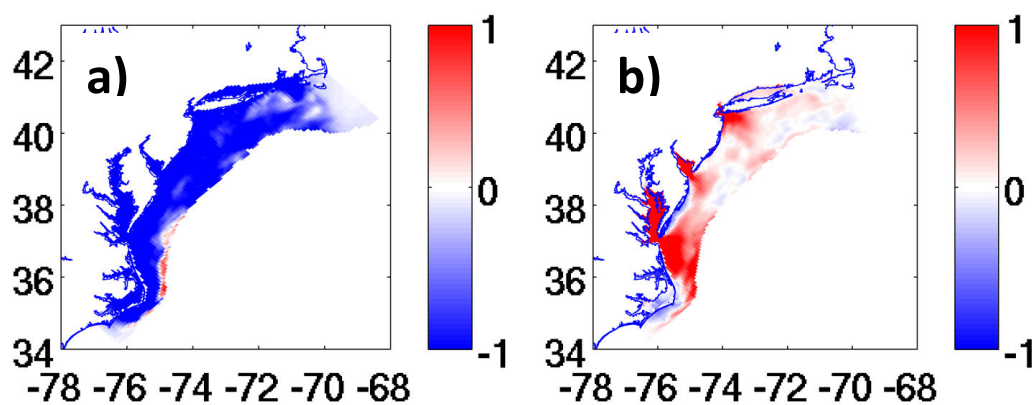


Figure 4. 6. The NCEP climatology temperature and salinity difference in January for the time period 1983-1986 and 2004-2008. a) temperature; b) salinity

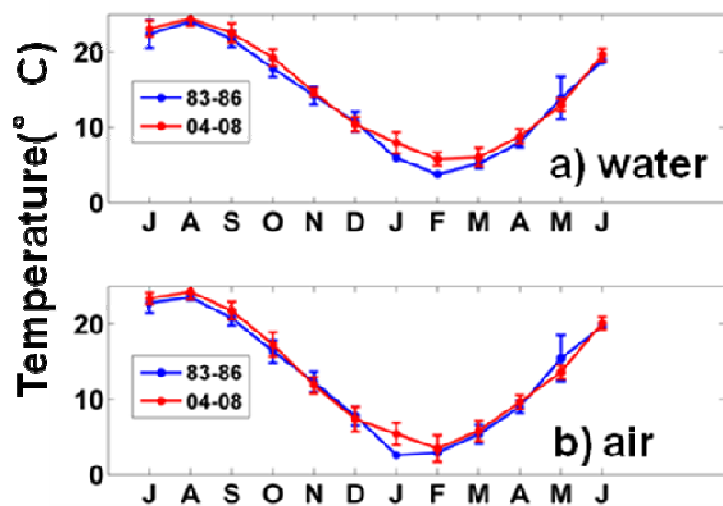


Figure 4. 7. The climatology water and air temperature of 44009 NDBC moored buoys for the time period of 1983-1986 and 2004-2008.

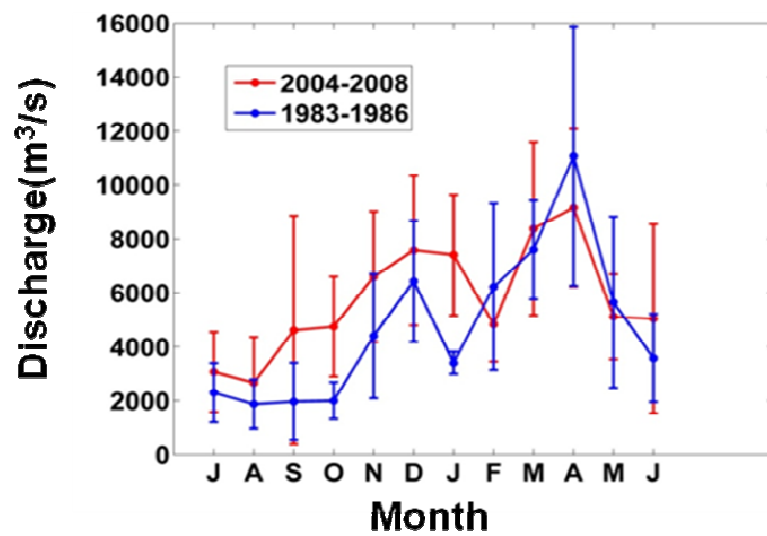


Figure 4. 8. The climatology of river discharge for the time period of 1983-1986 and 2004-2008.

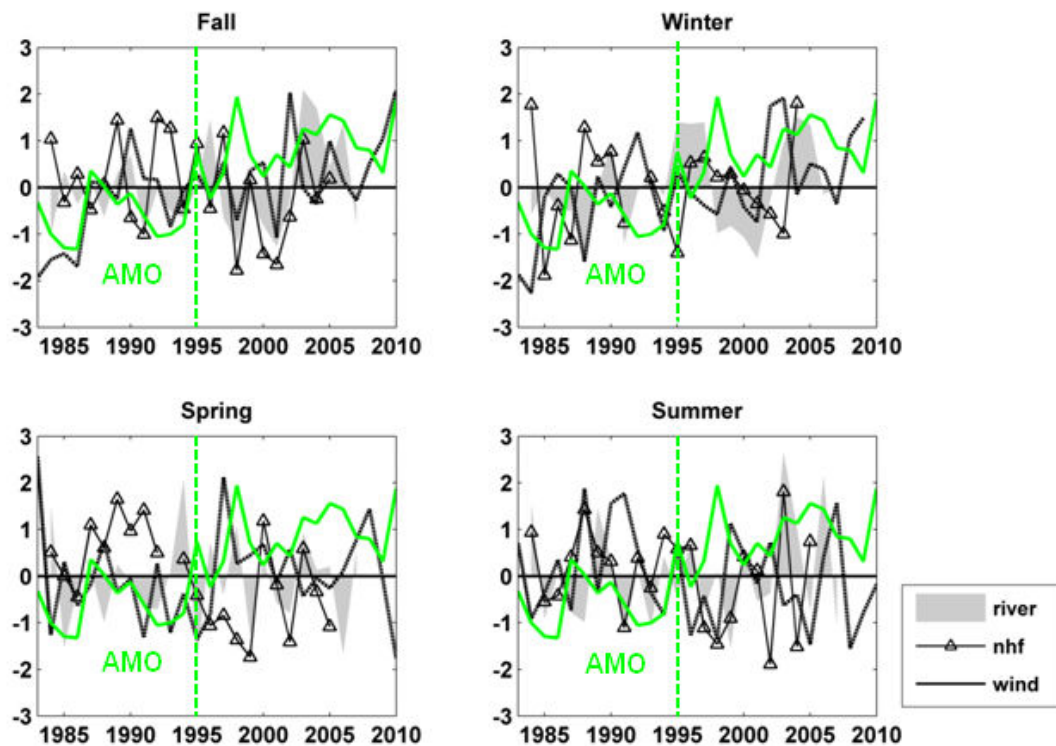


Figure 4. 9. Normalized anomalies of river, net heat flux and wind. The data are normalized by dividing the standard deviation of the time series. The AMO index is superimposed as green line. The year 1995 (vertical green line) is the division between the AMO- and AMO+.

CHAPTER 5. CONCLUSIONS

Through the analysis of satellite chlorophyll data, glider observations and bio-physical model in the MAB, this study characterized the phytoplankton dynamics and the dominant physical processes influencing phytoplankton blooms in shelf regions of MAB.

The EOFs analysis based on satellite chlorophyll confirm early research's view that an annual cycle common to MAB waters, consisting of a broad peak in mid-outer shelf region during winter and a relatively subtle across-shelf spring peaks. The shallow water winter bloom seems to be initiated by the breakup of the cold pool and persists throughout the winter under the condition of stable environment caused by winter fresh water stratification and only dies off when stratification is re-established. Inter-annual variability is evident and markedly influenced by events influencing water column stability like stormy weather conditions.

A three-dimensional high-resolution numerical model reproduced the seasonal bloom in the MAB and demonstrated the relationship between light and nutrients limitation for phytoplankton bloom. A critical mixing light value which results in the maximum chlorophyll biomass is used to parameterize the relative tradeoffs of mixing and light availability. The spatial variability of the critical light value was positively correlated with water depth. The model also diagnosed the wind-induced mixing, net heat flux, and river run off to be the key factors regulating water column stability so as to influencing phytoplankton bloom magnitude. Sensitivity model studies suggest that the timing of fall blooms is primarily associated with wind mixing, however, the magnitude of mid-winter bloom is more sensitive to water column stability which is influenced the

changes in fresh water runoff , ocean cooling/heating and wind mixing. The primary role of the rivers is to stabilize the water column other than bring nutrients to the shelf.

The studies of decadal variability of phytoplankton bloom based on CZCS and SeaWiFS chlorophyll and reveal that there is decreased of fall-winter bloom in the SeawiFs time period. NDBC weather data reveal that there is an increase trend of stormy frequency during winter for the period 1983 to 2010. This decrease of chlorophyll reflects shifts in the AMO from negative to positive mode that alters wind stress, river discharge, and net heat ocean flux.

REFERENCES

- Baldacci, A., Corsini, G., Grasso, R., Manzella, G., Allen, T.J., Cipollini, P., Guymer, H.T., Snaith, M.H., 2001. A study of the Alboran sea mesoscale system by means of empirical orthogonal function decomposition of satellite data. *Journal of Marine Systems* 29, 293 – 311.
- Barrick, D.E., 1972. First-order theory and analysis of mf/hf/vhf scatter from the sea. *IEEE Trans. Antennas Propag.* AP-20, 2 –10.
- Barrick, D.E., Evens, M.W., Weber, B.L., 1977. Ocean surface currents mapped by radar. *Science* 198, 138 – 144.
- Beardsley, R.C., Chapman, D.C., Brink, K.H., Ramp, S.R., Schlitz, R., 1985. The Nantucket Shoals flux experiment (NSFE79). Part I: A basic description of the current and temperature variability. *J. Phys. Oceanogr.*, 15, 713 – 748.
- Behrenfeld, M. J., Maranon, E., Siegel, D. A., Hooker, S. B., 2002. Photoacclimation and nutrient-based model of light-saturated photosynthesis for quantifying oceanic primary production. *Mar. Ecol. Prog. Ser.*, 228, 103– 117, doi:10.3354/meps228103.
- Biscaye, P.E., Flagg, C.N., Falkowski, P., 1994. The Shelf Edge Exchange Processes experiment, SEEP-II: an introduction to hypotheses, results and conclusions. *Deep-Sea Res. II* 41, 231– 252.
- Brickley, J.P., Thomas, C.A., 2004. Satellite-measured seasonal and inter-annual chlorophyll variability in the Northeast Pacific and Coastal Gulf of Alaska. *Deep-Sea Res. II*. 51, 229 – 245.
- Cahill, B., Schofield, O., Chant, R., Wilkin, J., Hunter, E., Glenn, S., Bissett, P., 2008. Dynamics of turbid buoyant plumes and the feedbacks on near-shore biogeochemistry and physics, *Geophysical Research Letters*, 35, L10605, doi:10.1029/2008GL033595.
- Campbell, J.W., 1995. The lognormal distribution as a model for bio-optical variability in the sea. *J. Geophys. Res.* 100, 13,237 – 13,254.
- Castelao, R., Glenn, S., Schofield, O., 2010. Temperature, salinity, and density variability in the central Middle Atlantic Bight. *J. Geophys. Res.*, 115. C10005, doi:10.1029/2009JC006082
- Castelao, R., Glenn, S., Schofield, O., Chant, R., Wilkin, J., Kohut, J., 2008b. Seasonal evolution of hydrographic fields in the central Middle Atlantic Bight from glider observations. *Geophys. Res. Lett.* 35, L03617, doi:10.1029/2007GL032335.
- Castelao, R., Schofield, O., Glenn, S., Chant, R., Kohut, J., 2008a. Cross-shelf transport of freshwater on the New Jersey shelf. *J. Geophys. Res.* 113, C07017, doi:10.1029/2007JC004241.

Chant, R.J., Wilkin, J., Zhang, W., Choi, B.J., Hunter, E., Castelao, R., Glenn, S., Jurisa, J., Schofield, O., Houghton, R., Kohut, J., Frazer, T., Moline, M., 2008b, Dispersal of the Hudson River Plume on the New York Bight. *Oceanography* 24, 55 – 63..

Chant, R.J., Glenn, S.M., Hunter, E., Kohut, J., Chen, R.F., Houghton, R.W., Bosch, J., Schofield, O., 2008a. Bulge Formation of a Buoyant River Outflow. *J. Geophys. Res.* 113, C01017, doi:10.1029/2007JC004100.

Crombie, D.D., 1955. Doppler spectrum of sea echo at 13.56 Mc/s. *Nature* 175, 681 – 682.

Cushing, D.H., 1975. *Marine Ecology and Fisheries* 278 pp., Cambridge Univ. Press, London.

Dickey, T.D., Williams III, A.J., 2001. Interdisciplinary ocean process studies on the New England shelf. *J. Geophys. Res.* 106, 9427 – 9434.

Dubinsky, Z., Schofield, O., 2010. From the light to the darkness: thriving at the light extremes in the oceans. *Hydrobiologia*, 639, 153–171.

Dutkiewicz, S., Follows, M., Marshall, J., Gregg, W. W., 2001. Interannual variability of phytoplankton abundances in the North Atlantic. *Deep Sea Res., Part II*, 48, 2323 – 2344, doi:10.1016/S0967-0645(00)00178-8.

Enfield, D. B., Mestas-Nunez, A. M., 1999. Multiscale variabilities in global SST and their relationships with tropospheric climate patterns, *J. Climate*, 12, 2719–2733.

Enfield, D. B., Luis, Cid-Serrano, 2010. Secular and multidecadal warmings in the North Atlantic and their relationships with major hurricane activity, *Int. J. Climate.*, 30 (2), 174–184.

Fairall, C. W., Bradley, E. F., Rogers, D. P., Edson, J. B., Young, G. S., 1996. Bulk parameterization of air-sea fluxes in TOGA COARE, *J. Geophys. Res.*, 101, 3747-3767.

Falkowski, P., Raven, J., 2007. *Aquatic Photosynthesis*, second ed. Princeton University Press, Princeton.

Fairall, C. W., Bradley, E. F., Hare, J. E., Grachev, A. A., Edson, J. B., 2003: Bulk parameterization of air-sea fluxes: updates and verification for the coare algorithm. *Journal of Climate*, 19 (4), 571–591.

Fasham, M. J. R., Ducklow, H. W., McKelvie, S. M., 1990. A nitrogen-based model of plankton dynamics in the oceanic mixed layer. *Journal of Marine Research* 48, 591–639.

Fennel, K., Wilkin, J., Levin, J., Moisan, J., O'Reilly, J., Haidvogel, D., 2006. Nitrogen cycling in the Middle Atlantic Bight: Results from a three-dimensional model and implications for the North Atlantic nitrogen budget. *Global Biogeochem., Cycles*, 20, GB3007, doi:10.1029/2005GB002456.

Field, C. B., Behrenfeld, M. J., Randerson, J. T., Falkowski, P., 1998. Primary production of the biosphere: Integrating terrestrial and oceanic components. *Science*, 281(5374), 237 – 240, doi:10.1126/science. 281.5374.237

Flagg, C. N., Wirick, C. D., Smith, S. I., 1994. The interaction of phytoplankton, zooplankton and currents from 15 months of continuous data in the Mid-Atlantic Bight. *Deep Sea Res., Part II*, 41, 411– 435.

Gentleman, W., Leising, A., Frost, B., Strom, S., Murray, J., 2003. Functional responses for zooplankton feeding on multiple resources: A review of assumption and biological dynamics. *Deep Sea Res., Part II*, 50, 2847– 2876.

Glenn, S.M., et al., 2004. Biogeochemical impact of summertime coastal upwelling on the New Jersey Shelf. *J. Geophys. Res.* 109, C12S02, doi: 10.1029/2003JC002265.

Glenn, S.M., Jones, C., Twardowski, M., Bowers, L., Kerfoot, J., Webb, D., Schofield, O., 2008. Glider observations of sediment resuspension in a Middle Atlantic Bight fall transition storm, *Limnol. Oceanogr.*, 53, 2180 – 2196.

Gong, D., Kohut, J.T., Glenn, S.M., 2010. Wind driven circulation and seasonal climatology of surface current on the NJ Shelf (2002–2007). in press.

Haidvogel, D. B., Beckmann, A., 1999. *Numerical Ocean Circulation Modeling*, Ser. Environ. Sci. Manage., vol. 2, 318 pp., Imp. Coll. Press, London.

Harding, W.L., Magnuson, A., Mallonee, M.E., 2004. SeaWiFS retrievals of chlorophyll in Chesapeake Bay and the mid-Atlantic bight. *Estuar. Coast. Shelf Sci.* 62, 75 – 94.

Henson, A.S., Robinson, I. Allen, J.T., Waniek, J.J., 2006. Effect of meteorological conditions on interannual variability in timing and magnitude of the spring bloom in the Irminger Basin, North Atlantic. *Deep-Sea Res. I* 53, 1601 – 1615.

Kerr, R. A., 2000. A North Atlantic climate pacemaker for the centuries, *Science*, 288 (5473), 1984-1986.

Hofmann, E. E., Cahill, B., Fennel, K., Friedrichs, M. A. M., Hyde, K., Lee, C., Mannino, A., Najjar, R. G., O'Reilly, J. E., Wilkin J., Xue, J., 2011. Modeling the dynamics of continental shelf carbon. *Annual Review of Marine Science*, 3, 93 -122.

Houghton, R., Schlitz, R., Beardsley, R., Butman, B., Chamberlin, J., 1982. The middle Atlantic Bight cold pool: Evolution of the temperature structure during summer 1979. *J. Geophys. Res.* 12, 1019 – 1029.

Howarth, et al., 1996. Regional nitrogen budgets and riverine N & P fluxes for the drainages to the North Atlantic Ocean: Natural and human influences. *Biogeochemistry*, 35, 181-226.

- Huisman, J., Jonker, R. R., Zonneveld, C., Weissing, F. J., 1999b. Competition for light between phytoplankton species: experimental tests of mechanistic theory. *Ecology*, 80, 211–222.
- Huisman, J., Van, O.P., Weissing, F.J., 1999a. Critical depth and critical turbulence: Two different mechanisms for the development of phytoplankton blooms. *Limnol. Oceanogr.* 44, 1781 – 1787.
- Irigoiien, X., Castel, J., 1997. Light limitation and distribution of chlorophyll pigments in a highly turbid estuary: the Gironde (SW France). *Estuarine, Coastal and Shelf Science* 44, 507–517.
- Ji, R., Davis, C.S., Chen, C., Townsend, D.W., Mountain, D.G., and Beardsley, R.C., 2007. Influence of ocean freshening on shelf phytoplankton dynamics. *Geophys. Res. Lett.* 34, L24607.
- Johnson, D.M., Miller, J., Schofield, O., 2003. Dynamics and optics of the Hudson River outflow plume. *J. Geophys. Res.* 108, 1–9.
- Kohut, J.T., and Glenn, S.M., 2003. Calibration of HF radar surface current measurements using measured antenna beam patterns. *J. Atmos. Oceanic Technol.* 1303 – 1316.
- Kohut, J.T., Glenn, S.M., Chant, R.J., 2004. Seasonal current variability on the New Jersey inner shelf. *J. Geophys. Res.* 109, C07S07, doi: 10.1029/2003JC001963.
- Lentz, S., Shearman, K., Anderson, S., Plueddemann, A., Edson, J., 2003. Evolution of stratification over the New England shelf during the Coastal Mixing and Optics study, August 1996–June 1997. *J. Geophys. Res.*, 108(C1), 3008, doi: 10.1029/2001JC001121.
- Linder, C.A., Gawarkiewicz, G., 1998. A climatology of the shelf-break front in the
- Linder, C.A., Gawarkiewicz, G., Pickart, R., 2004. Seasonal characteristics of bottom boundary layer detachment at the shelfbreak front in the Middle Atlantic Bight. *J. Geophys. Res.* 109, C03049, doi: 10.1029/2003JC002032.
- Longhurst, A. R., 1998. *Ecological Geography of the Sea*. 398 pp., Academic Press, San Diego.
- Lorenz, E.N., 1956. Empirical orthogonal functions and statistical weather prediction. *Sci. Rep. No. 1*, 49 pp., *Statist. Forecasting Proj.*, Department Meteor., MIT.
- Malone, T.C., Hopkins, T.S., Falkowski, P.G., Whitedge, T.E., 1983. Production and transport of phytoplankton biomass over the continental shelf of the New York Bight. *Cont. Shelf Res.* 1, 305 – 337.
- Martin, H. J., 1965. Phytoplankton-zooplankton relationships in Narragansett Bay. *Limnol. oceanogr.*, 10, 185–191.

- Martinez, E., Antoine, D., Ortensoi, F. D, Gentili, B., 2009. Climate-driven basin-scale decadal oscillations of oceanic phytoplankton, *Science*, 326, 1253-1256.
- Mesinger, F., and Coauthors, 2006. North American Regional Reanalysis. *Bull. Amer. Meteor. Soc.*, 87, 343–360.
- Mobley, C.D., 1994. *Light and Water, Radiative Transfer in Natural Waters*. Academic Press, California.
- Moline, M. A., Blackwell, S., Chant, R., Oliver, M. J., Bergmann, T., Glenn, S., Schofield, O., 2004. Episodic physical forcing and the structure of phytoplankton communities in the coastal waters of New Jersey, *J. Geophys. Res.*, 110, C12S05, doi:10.1029/2003JC001985.
- Moline, M.A., Frazer, T.K., Chant, R., Glenn, S., Jacoby, C.A., Reinfelder, J.R., Yost, J., Zhou, M., and Schofield, O., 2008. Biological responses in a dynamic, buoyant river plume. *Oceanography* 21, 71 – 89.
- Mountain, D.G., 2003. Variability in the properties of Shelf Water in the Middle Atlantic Bight, 1977–1999. *J. Geophys. Res.* 108(C1), 3014, doi: 10.1029/2001JC001044.
- Nantucket Shoals flux experiment (NSFE79). Part I: A basic description of the current and temperature variability. *J. Phys. Oceanogr.* 15, 713 – 748.
- Navarro, G., Ruiz, J., 2006. Spatial and temporal variability of phytoplankton in the Gulf of Cadiz through remote sensing images. *Deep-Sea Res. II* 53, 1241–1260.
- North, G.R., Bell, T.L., Cahalan, R.F., and Moeng, F.J., 1982. Sampling errors in the estimation of empirical orthogonal functions. *Mon. Weather Rev.* 110, 699 – 706.
- O'Reilly J., Busch, D., 1984. Phytoplankton primary production on the north-west Atlantic Shelf, *Rapports et Proces-Verbaux des Reunions Conseil International pour l'Exploration de la Mer.* 183, 255 – 268.
- Obate, A., Ishizake, J., Endoh, M., 1996. Global verification of critical depth theory for phytoplankton bloom with climatological in situ temperature and satellite ocean color data. *J. Geophys. Res.*, 101, 20657-20667.
- O'Reilly, J., Evans-Zetlin E. C., Busch, D. A., 1987. Primary Production. 220-233. In R. H. Backus and D. W. Bourne [eds.], *Georges Bank*. MIT Press.
- O'Reilly, J., Zetlin, C., 1998. Seasonal, horizontal, and vertical distribution of phytoplankton chlorophyll a in the northeast U.S. continental shelf ecosystem. NOAA Technical Report NMFS 139. U.S. Department of Commerce.
- Pawlowicz, R., Beardsley, R.C., Lentz, S.J., 2002. Classical Tidal Harmonic Analysis Including Error Estimates in MATLAB using T TIDE. *Computers and Geosciences* 28, 929 – 937
- Riley, G.A., 1946. Factors controlling phytoplankton populations on Georges Bank. *J. Mar. Res.* 6, 54 – 73.

Riley, G.A., 1947. Seasonal fluctuations of the phytoplankton population in New England coastal waters. *J. Mar. Res.* 6, 114 – 125.

Ryan, J. P., Yoder, J. A., Cornillon, P. C., 1999. Enhanced Chlorophyll at the Shelfbreak of the Mid-Atlantic Bight and Georges Bank during the Spring Transition. *Limnol. Oceanogr.*, 44, 1 – 11.

Ryan, J.P., Yoder, J.A., Townsend, D.W., 2001. Influence of a Gulf Stream warm-core ring on water mass and chlorophyll distributions along the southern flank of Georges Bank. *Deep-Sea Res. II*, 48, 159-178.

Ryther, J.H., Yentsch, C.S., 1958. Primary production of continental shelf waters off New York. *Limnol. Oceanogr.* 3, 327 – 335.

Schofield, O., Bergmann, T., Oliver, M., Irwin, A., Kirkpatrick, G., Bissett, W. P., Orrico, C., Moline, M. A., 2004. Inverting inherent optical signatures in the nearshore coastal waters at the Long Term Ecosystem Observatory. *J. Geophys. Res.*, 109, C12S04, doi:10.1029/2003JC002071.

Schofield, O., Chant, R., Cahill, B., Castelao, R., Gong, D., Kohut, J., Montes-Hugo, M., Ramanduri, R., Xu, Y., Glenn, S., 2008. Seasonal forcing of primary productivity on broad continental shelves. *Oceanography* 21, 108 – 117.

Schofield, O., Chant, R., Hunter, E., Moline, M. A., Reinfelder, J., Glenn, S. M., Frazer, T. Optical transformations in a turbid buoyant plume. *Cont. Shelf Res.*, (submitted)

Schofield, O., et al., 2007. Slocum gliders: Robust and ready. *J. Field Robotics* 24, 1 –14, doi: 10.1009/rob.20200.

Schofield, O., et al., 2010. Automated sensor networks to advance ocean science . *Transaction of the American Geophysical Union* 91(39): 345-346. doi:10.1029/2010EO390001.

Shearman, R. K., and S. J. Lentz, 2010. Long-term sea surface temperature variability along the U.S. East Coast, *J. Phys. Oceanogr.*, 40, 1004 –1017.

Siedlecki, S.A., Mahadevan, A., Archer, D., 2008. The Role of Shelf Break Upwelling Along the East Coast of the US in the Coastal Carbon Cycle: A Model's Tale. *American Geophysical Union, Fall Meeting 2008*, poster #OS53C-1322.

Siegel, D. A., Doney, S. C., Yoder, J. A., 2002. The North Atlantic spring phytoplankton bloom and Sverdrup's critical depth hypothesis. *Science*, 296, 730 – 733.

Simpson, J. H., Hughes, D. G., Morris, N. C. G., 1977. The relation of seasonal stratification to tidal mixing on the continental shelf. *A Voyage to Discovery. Deep-Sea Research (Suppl.)*, 327–340.

Simpson, J. H., Bowers, D., 1981. Models of stratification and frontal movement in shelf seas. *Deep-Sea Research* 28A, 727–738.

Smetacek, V., Passow, U., 1990. Spring bloom initiation and Sverdrup's critical depth model. *Limnol. Oceanogr.*, 35 (1), 228–234.

Stewart, R.H., Joy, J.W., 1974. HF radio measurement of surface currents. *Deep-Sea Res.* 21, 1039 – 1049.

Stramska, M., Dickey, T., 1994. Modeling phytoplankton dynamics in the northeast Atlantic during the initiation of the spring bloom. *J. Geophys. Res.* 99, 10,241 – 10,253.

Summer 1979. *J. Geophys. Res.* 12, 1019 – 1029.

Sverdrup, H. U., 1953. On conditions for the vernal blooming of phytoplankton. *J. Cons. Perm. Int. Exp. Mer.* 18, 287 – 295.

Tilman, D., 1982. Resource competition and community structure. Princeton University Press, Princeton, NJ, U.S.A.

Townsend, D.W., Cammen, L.M., Holligan, P.M., Campbell, D.E., Pettigrew, N.R., 1994. Causes and consequences of variability in the timing of spring phytoplankton blooms. *Deep-Sea Res. I* 41, 747 – 765.

Townsend, D.W., Keller, M.D., Sieracki, M.E., Ackleson, S.G., 1992. Spring phytoplankton blooms in the absence of vertical water column stratification. *Nature* 360, 59 – 62.

Turner, J. T., Tester, P. A., 1997. Toxic marine phytoplankton, zooplankton grazers, and pelagic food webs. *Limnol. Oceanogr.*, 42, 1203-1214.

Ward, J.H., 1963. Hierarchical grouping to optimize an objective function. *J. Am. Statist. Assoc.* 58, 236 – 244.

Wilkin, J. L., Arango, H. G., Haidvogel, D. B., Lichtenwalner, C. S., Glenn, S. M., Hedstrom, K. S., 2005. A regional ocean modeling system for the Long-term Ecosystem Observatory. *J. Geophys. Res.*, 110, C06S91, doi:10.1029/2003JC002218.

Wright, W.R., 1976. The limits of shelf water south of Cape Cod, 1941–1972. *J. Mar. Res.* 34, 1 – 14.

Xu, Y., Chant, R., Gong, D., Castelao, R., Glenn, S., Schofield, O., 2011. Seasonal variability of chlorophyll a in the Mid-Atlantic Bight. *Cont. Shelf Res.*, doi:10.1016/j.csr.2011.05.019..

Xu, Y., Cahill, B., Wilkin, J., Schofield, O., 2012. Role of wind in regulating phytoplankton blooms on the Mid-Atlantic Bight, *Cont. Shelf Res.*, in press.

Yoder, J.A., McClain, C.R., Feldman, G.C., Esaias, W.E., 1993. Annual cycles of phytoplankton chlorophyll concentrations in the global ocean: A satellite view. *Global Biogeochemical Cycles* 7, 181 – 194.

Yoder, J. A., O'Reilly, J. E., Barnard, A. H., Moore, T. S., Ruhsam, C. M., 2001. Variability in coastal zone color scanner (CZCS) Chlorophyll imagery of ocean margin waters off the US East Coast. *Cont. Shelf Res.*, 21, 1191 – 1218.

Yoder, J.A., Schollaert, S.E., O'Reilly, J.E., 2002. Climatological Phytoplankton Chlorophyll and Sea Surface Temperature Patterns in Continental Shelf and Slope Waters off the Northeast U.S. Coast. *Limnol. Oceanogr.* 3, 672 – 682.

Curriculum Vita

Yi Xu

EDUCATION

- 2006-Pres. Ph.D. candidate (expect to graduate in October, 2012), Oceanography, Rutgers University, New Brunswick, New Jersey
- 2003-2006 M.S. Physical Oceanography, First Institute of Oceanography, Key Laboratory of Marine Science and Numerical Modeling, Qingdao, China
- 1999-2003 B.S. Atmospheric Science, Ocean University of China, Qingdao, China

RESEARCH INTERESTS

Numerical ocean modeling, Air-sea interaction, phytoplankton dynamics, nutrients budget, bio- physical interaction, climate change and the oceans dynamics.

RESEARCH EXPERIENCE

- 2006 – Pres. Research Assistant, Coastal Ocean Observations Lab, Rutgers University
- Data analysis of AVHRR sea surface temperature and SeaWiFS CZCS chlorophyll, Webb Slocum Glider and High Frequency Radom (CODAR) data sets.
 - Study the ocean circulation and bio-physical interaction in the continental shelves of North America based on ROMS. Specifically focus on the influence of wind mixing and river run off on nutrient cycle and phytoplankton bloom in the coastal area.
 - Model sensitivity studies to test the respond of model variables under different forcing condition. Model optimizations.
- 2004 – 2006 Research assistant, Key Laboratory of Marine Sciences and Numerical Modeling, First Institute of Oceanography, P. R. China
- Statistical analysis of satellite sea surface temperature (SST) data.
 - Numerical simulation of physical field based on ECOMSED Model. Model calibration and validation.
 - Coupling water quality model (RCA) to ECOMSED to study the nutrient cycle and biophysical interaction.
- 2003 Research Assistant, Ocean University of China

- Data mining and Statistical analysis of model reanalysis data in Matlab and FORTRAN

PUBLICATIONS

- Y. Xu, Chant, R., and Schofield, O. Decadal Variability of Climate and Phytoplankton Bloom in the Mid-Atlantic Bight. *Geophysical research letters*, in prepare.
- Y. Xu, Cahill, B., Wilkins, J., and Schofield, O. Regulation of the phytoplankton bloom on the Mid-Atlantic Bight by wind mixing. *Continental shelf research*, in review.
- Y. Xu, Robert Chant, Donglai Gong, Renato Castelao, Scott Glenn and Oscar Schofield 2011. Seasonal variability of chlorophyll a in the Mid-Atlantic Bight. *Continental shelf research*, doi:10.1016/j.csr.2011.05.019.
- Schofield, O., R. Chant, B. Cahill, R. Castelao, D. Gong, J. Kohut, M. Montes-Hugo, R. Ramanduri, Y. Xu, and S. Glenn, 2008. The decadal view of the Mid-Atlantic Bight from the COOLroom: Is our coastal system changing? *Oceanography*, 21, 108 – 117.
- Y. Xu, F. Yu, X. Zhang, 2005. Diagnostic Calculation of Yellow Sea Warm Current in winter. *Advance in Marine Science*, 23(4): 398-407.
- Yu F., Y. Xu, 2003. Study of Long-term Variational Trend of Sea Surface Temperature in the East China Sea. *Advance in Marine Science*, 21(4): 477-481.

PRESENTATIONS AND POSTERS:

- The wind mixing for the regulation of the phytoplankton bloom on the Mid-Atlantic Bight. Y. Xu, Cahill, B., Wilkins, J., and Schofield, O., ASLO Aquatic Sciences Meeting, 2011, San Juan, Puerto Rico. (GS08A Plankton Ecology, talk)
- Role of water column stability in regulating phytoplankton blooms in the Mid-Atlantic Bight. Y. Xu; B. E. Cahill, R. Chant, O. Schofield, *Ocean Sciences* 2010, Portland, OR (BO13C-07, talk)
- Spring time in Winter: Phytoplankton Dynamics on the Middle Atlantic Bight. Y. Xu, Schofield O., Chant, R., and Glenn S., *Ocean Sciences* 2008, Orlando, FL. (Abstract OS)
- Spring time in Winter: Phytoplankton Dynamics on the Middle Atlantic Bight Y. Xu, Schofield O., Chant, R., and Glenn S., *Mid-Atlantic Bight Physical Oceanography Meeting*, Woods Hole, MA, 2008 (poster)

EDUCATIONAL EXPERIENCE

2011 Teaching Assistant, *Oceanographic Methods and Data Analysis*.

2009 Teaching Assistant, *Oceanographic Methods and Data Analysis*.

HONORS & PROFESSIONAL AFFILIATIONS

2007-2008: Vice President of Oceanography Graduate Students Association, IMCS,
Rutgers University.

2003-2006: Excellent Graduate Student Fellowship, First Institute of Oceanography.

2001-2002: President of Publication Union, Marine and Environment Department,
Ocean University of China.